TR-ACR-0005

Ground Skirt Monopole Array Antenna Far Field Analysis
Based on an Equivalent Weight Vector Approximation

Helena Jacob, Qing Han,

Keizo Inagaki and Takashi Ohira

2002.9.30

ABSTRACT

This paper proposes a way of simulating an adaptative array antenna, named the ESPAR antenna using HFSS software. The model that has been achieved for this simulation is proved to be accurate as for each set of reactances obtained by experimental beamforming, far field directivity patterns has been obtained similar to the experimental ones. Furthermore, Equivalent Weight Vector approximation based on reactive near field approach is also studied. The patterns obtained by conventional far field method and those obtained by this approximation show good agreements when increasing the number of points picked up on the antenna to calculate this approximation. Therefore, efforts and time can be saved thanks to this new way of characterizing the ESPAR antenna, that is easier and more economical than the experimental one. Eventually, this Simulation technique can also be used in the future to optimize the ESPAR antenna, by improving the algorithms that adaptatively control the set of reactances, which is still a hot topic.

ACKNOWLEDGEMENTS

Contents

List of Figures

9

List of Tables

Glossary and Key words

ATR : Advanced Telecommunications Research International Institute

ACR : Adaptative Communications Research Laboratory

ENSSAT : École Nationale Supérieure de Sciences Appliquées et de Technologie

ESPAR : Electronicaly Steerable Parasitic Array Radiator

Adaptative Array Antenna : antenna which architecture operating principle is based upon electromagnetic coupling among array elements where the array is reactively controlled

Anechoic Chamber : chamber without echo, i.e. absorbing, so that a reduction of reflection that would otherwise compromise measurements accuracy is achieved

Far Field : the region where the antenna patterns need to be measured with adequate transmission distance (in terms of wavelength) or they will not be typical of the patterns expected in typical use over long distance. The wave is there known to be a plane wave, and the electromagnetic energy decays in $\frac{1}{r}$

Near Field : Measurements made over short distances (near field) contain errors because the fields are curved rather than planar. The electromagnetic energy decays in $\frac{1}{r^2}$

Reactive Near Field : region nearest to the antenna, also known as evanescent region. Its component of the electromagnetic energy decays very rapidly with distances ($\frac{1}{r^3}$). Near field measurements are generally made outside the evanescent region, except in our case

EWV : Equivalent Weight Vector approximation, based on reactive near field measurements

WACNet : Wireless Ad-Hoc Commmunity Network

FEM : Finite Element Method

IEICE : Institute of Electronics, Information and Communication Engineers

Directivity Pattern : also known as Radiation pattern, refers to the variation of the radiated field strength (or received signal level) found as the studied antenna is rotated

Omni Pattern : radiation pattern where the intensity of the radiated field is the same in all directions

Beam Pattern : radiation pattern where the intensity of the radiated field is maximum in one chosen direction

GSM : Global System for Mobile Communication

PHS : Personal Handy Phone System

Wireless LAN : Wireless Local Area Network, also known as the IEEE 802.11 norm

DBF : Digital Beam Forming

RF : Radio Frequency

HFSS : High Frequency Structure Simulator

TEM : Transverse ElectroMagnetic Wave

DAC : Digital Analog Converter

RFAB : Reactive Field Anechoic Box

S-parameter : Scattering parameters, amplitude and phase of the incoming wave on a transmission line, which is "scattered" by the circuit and its energy is partitioned between all the possible outgoing waves on all the other transmission lines connected to the circuit. Fixed properties which describe how the energy couples between each pair of ports or transmission lines connected to the circuit

CAD : Computer-Aided Drawing

DoA : Direction of Arrivals

RLC : Resistance Inductance(L) Capacitance

OS : Operating System

Key words : ESPAR antenna, array antenna, far field pattern, reactive near field approach, Equivalent Weigth Vector approximation, HFSS

14

INTRODUCTION

As the amount of wireless communications is increasing from day to day, and with it, the functionalities brought to users, communication systems has to face to higher constraints of bandwidth and data rates. Moreover, in the case of mobile terminals studies, power consumption and device sizes are also hot topics, as the aim is to obtain a high quality of signal transmission while decreasing the cost and sizes of the components used in those devices.

ATR-Adaptative Communications Research Laboratories has proposed a Wireless Ad-Hoc Community Network (WACNet) concept, which aim is to form an ad-hoc community, that is to say to create a temporary network among an unspecified number of people that have a common purpose. For this WACNet, a specific antenna is needed, which is able to adaptatively form beams and nulls. The Electronically Steerable Parasitic Adaptative Radiator (ESPAR), a reactively controlled directive antenna that enables full azimuth directivity, is actually studied in ACR-Departement 3, as a low cost, low power consumption and high power level device.

In order to find adaptative algorithms to control the ESPAR antenna directivity, characterization and calibration of the antenna and its reactances are needed. Characterization is already possible by getting radiation patterns, but the conventional experimental method achieved using large anechoic chamber costs great time and efforts. A reactive near field method to get far field directivity patterns by measuring the current only at discrete points picked up in the evanescent region of the antenna has been presented, using experimental techniques. The purpose of this internship has been to study, by Simulation, the Equivalent Weight Vector approximation based on this reactive near field approach and to find the optimum number of points picked up on the antenna to get the far field, still using simulation.

After presenting the ATR Adaptative Communications Research Laboratories, and the WACNet concept, the ESPAR antenna will be introduced. Then, the purpose and background of the project will be presented. Eventually, the simulation of conventional far field and reactive near field methods and their comparison will be developed.

Chapter 1

Introduction to the ESPAR Antenna

1.1 Theory on ESPAR antenna

1.1.1 Adaptative Array Antenna

In modern wireless communication systems, cochannel interferences become a dominant factor in limiting quality and capacity. The adaptative array antenna is an emerging technology that has gained much attention over the last few years for its ability to significantly increase the performance of wireless systems by effectively suppressing these cochannel interferences. While the wireless community has paid a great deal of attention to adaptative systems for base stations, relatively little effort has been focused on how to improve *mobile user terminals* using advanced adaptative antenna techniques.

Mobile user terminal applications have stringent limitations on hardware and algorithm complexity as well as power consumption. Indeed, it is well known that nearly all-existing antenna array techniques, that is to say Digital Beam Forming (DBF) architectures, required one receiver per branch of antenna (cf. Figure 1.1). For a two-elements array antenna for instance, this doubles the receiver hardware and is not an easy trade-off to make where it is essential to reduce system complexity.

For the reasons of hardware, complexity, power consumption, etc., no conventional DBF array antenna, which multiplies the receiver hardware by the number of branches, is a suitable candidate for low-power mobile user terminal applications.

1.1.2 ESPAR antenna: Electronically Steerable Parasitic Array Radiator antenna

Analog adaptative beamformers, e.g., Electronically Steerable Parasitic Array Radiator (ESPAR) antennae, have shown the potential for application
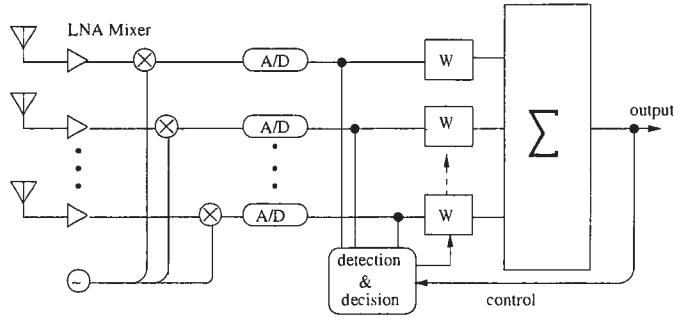
Figure 1.1: Diagram of a conventional array antenna

to wireless communication systems, and especially to *mobile user terminals* as small-sized, high-performance antennae featuring a directivity able to be controlled at low cost with small power consumption. The $(M+1)$-elements ESPAR antenna, as depicted in Figure 1.2 where $M = 6$, has *only an active radiator* (the 0-th element) connected to the receiver. The remaining M elements, which are grounded through varactors (variable reactors), are passive. Variable reactances of the varactors, controlled by bias voltages, alter the performance of the antenna so that directional beams or nulls can be steered through 360° azimuth.
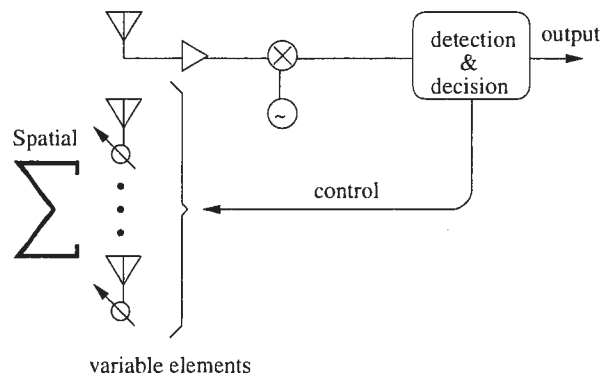
Figure 1.2: Diagram of an adaptive ESPAR antenna

1.1.3   ESPAR antenna: Formulation

In this section, we briefly describe the basic configuration and give the formulation of the ESPAR antenna[4]. The frequency of the antenna studied is 2.484 GHz ($\lambda = 12.07cm$). All the elements are slightly shorter than 0.25λ mounted on a circle ground with a radius of 0.5λ to obtain resonance

at the desired frequency (cf. Figure 1.3). A skirting is used on a finite ground plane structure to reduce the main lobe elevation[5]. The values $x_m(m = 1, 2, \ldots, M)$ of the reactances, that can change the pattern of the antenna, may be constrained in practical applications in certain ranges, e.g., from -300Ω to 300Ω. The vector denoted by
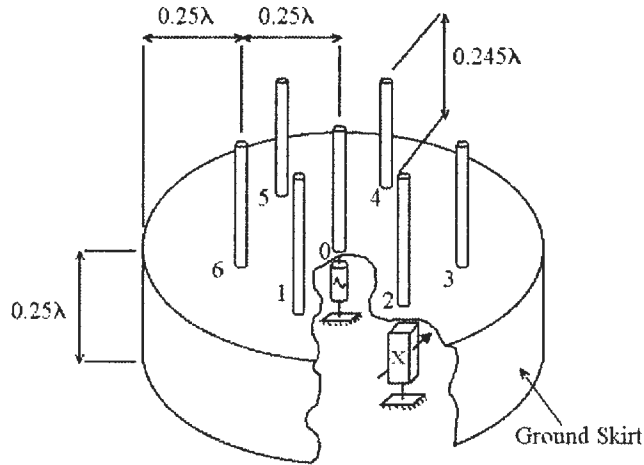
Figure 1.3: ESPAR antenna

$$\mathbf{x} \overset{\triangle}{=} [x_1, x_2, \ldots, x_M]^T \tag{1.1}$$

is called the *reactance vector* or *set of reactances*, which is variable, and thus is used to form the antenna pattern. The superscript ^{T} is the transpose of the vector or matrix.

We now briefly formulate the output of the ESPAR antenna that is a function of these M reactances[4, 6]. Denote $\mathbf{s(t)} = [s_0(t), s_1(t), \ldots, s_M(t)]^T$, where the component $s_m(t)$ is the RF signal impinging on the $m-th$ element of the ESPAR antenna. Then, the single-port RF output $y(t)$ of the antenna is given by

$$y(t) = \mathbf{i}^T \mathbf{s}(t), \tag{1.2}$$

where $\mathbf{i} = [i_0, i_1, \ldots, i_M]^T$ is the RF current vector with the component i_m appearing on the $m - th$ element. Next we give a representation of the current vector as a function of the reactance vector (cf. equation (1.7))[4]. For convenience, we derive the representation under the assumption that the ESPAR antenna is operating in a transmit mode. The theorem of reciprocity tells us that the receive-mode radiation pattern of an antenna is equal to that of the transmit-mode. Therefore the representation of equation (1.7) is also available in the receive-mode.

Denote by $\mathbf{v} = [v_0, v_1, \ldots, v_M]^T$ the RF voltage vector, where

$$v_m = -jx_m i_m, \qquad m = 1, 2, \ldots, M, \qquad (1.3)$$

is the RF voltage imposed on the reactance x_m, and

$$v_0 = V_s - Z_0 i_0, \qquad (1.4)$$

is the RF voltage at the central element[4]. The notation Z_0 is the output impedance of the transmitter (or the impedance of the receiver in the receiver-mode), and is not influenced by the mutual coupling of elements. The value of Z_0 is assumed to be 50Ω without loss of generality. In equation (1.4), V_s is the internal source voltage of the transmitter. According to the theorem of reciprocity, the receive-mode radiation pattern or array-factor of the ESPAR antenna is the same as that of the transmit-mode. Once obtained, the array factor is not affected by V_s. Thus we assume $V_s = 1$ without loss of generality. Arranging equations (1.3) and (1.4) in a vector form yields

$$\mathbf{v} = \begin{bmatrix} 1 - 50i_0 \\ -jx_1 i_1 \\ -jx_2 i_2 \\ \vdots \\ -jx_M i_M \end{bmatrix} = \begin{bmatrix} 1 \\ 0 \\ 0 \\ \vdots \\ 0 \end{bmatrix} - \mathbf{Xi}, \qquad (1.5)$$

where $\mathbf{i} = [i_0, i_1, \ldots, i_M]^T$, and the diagonal matrix

$$\mathbf{X} = diag[50, jx_1, jx_2, \ldots, jx_M]$$

is called the reactance matrix.

On the other hand, the RF current vector $\mathbf{i}$ and RF voltage vector $\mathbf{v}$ have the relationship

$$\mathbf{i} = \mathbf{Yv}, \qquad (1.6)$$

where $\mathbf{Y} = [y_{kl}]_{(M+1) \times (M+1)}$ is referred as to the admittance matrix, where y_{kl} expresses the mutual admittance between the element k and l ($0 \leq k, l \leq M$).

Substituting (1.5) into (1.6) yields

$$\mathbf{i} = (\mathbf{I} + \mathbf{YX})^{-1}\mathbf{y_0}, \qquad (1.7)$$

where $\mathbf{I}$ is the identity matrix of order $M + 1$, and the vector

$$\mathbf{y_0} = [y_{00}, y_{10}, y_{20}, \ldots, y_{M0}]^T \qquad (1.8)$$

is the first column of $\mathbf{Y}$.

For the $(M + 1)$-elements ESPAR antenna with $M = 6$, the vector $\mathbf{y_0}$ and the admittance matrix $\mathbf{Y}$ are determined by only 6 components of the mutual admittance[4], which is explained as follows.

By the reciprocity theorem, it holds, similarly to conventional array antennae, that

$$y_{kl} = y_{lk} \qquad (1.9)$$

Furthermore, the cyclic symmetry of the elements of the ESPAR antenna implies

$$
\begin{aligned}
y_{11} &= y_{22} = y_{33} = y_{44} = y_{55} = y_{66}, \\
y_{01} &= y_{02} = y_{03} = y_{04} = y_{05} = y_{06}, \\
y_{12} &= y_{23} = y_{34} = y_{45} = y_{56} = y_{61}, \\
y_{13} &= y_{24} = y_{35} = y_{46} = y_{51} = y_{62}, \\
y_{14} &= y_{25} = y_{36}.
\end{aligned}
\qquad (1.10)
$$

Equations (1.9) and (1.10) above imply that the admittance matrix $\mathbf{Y} = [y_{kl}]_{(M+1)\times(M+1)}$ is determined by only 6 components of the mutual admittances $y_{00}, y_{10}, y_{11}, y_{21}, y_{31}, y_{41}$. The values of the 6 components depend on the physical structure of the antenna, e.g., the radius, the space intervals and the lengths of the elements, and therefore are constants. Summarizing the above explanation, we write the admittance matrix $\mathbf{Y}$ in equation (1.7) as

$$
\mathbf{Y} =
\begin{bmatrix}
y_{00} & y_{10} & y_{10} & y_{10} & y_{10} & y_{10} & y_{10} \\
y_{10} & y_{11} & y_{21} & y_{31} & y_{41} & y_{31} & y_{21} \\
y_{10} & y_{21} & y_{11} & y_{21} & y_{31} & y_{41} & y_{31} \\
y_{10} & y_{31} & y_{21} & y_{11} & y_{21} & y_{31} & y_{41} \\
y_{10} & y_{41} & y_{31} & y_{21} & y_{11} & y_{21} & y_{31} \\
y_{10} & y_{31} & y_{41} & y_{31} & y_{21} & y_{11} & y_{21} \\
y_{10} & y_{21} & y_{31} & y_{41} & y_{31} & y_{21} & y_{11}
\end{bmatrix}
$$

Similarly, equation (1.8) can be rewritten as

$$
\mathbf{y_o} = [y_{00}, y_{10}, y_{10}, \ldots, y_{10}]^{T}.
$$

1.2 Characterization of ESPAR antenna

The purpose

Antennae like the ESPAR antenna, that directly integrate semiconductor devices, are problematic due to the occurrence of semiconductor device installation errors. Therefore, antenna characteristics such as *radiation patterns* may differ from antenna to antenna. The purpose of this part of the global ESPAR antenna Project is then to obtain consistent antenna characteristics.

There exists a method of repeated far field pattern measurements with adjustment of varactor control voltages[8]. However, this method is time consuming and cannot give the current distribution on the ESPAR antenna elements. Accordingly, we want to develop a more simple method of *calibrating the reactance values using the control voltages*. The story is shown on Figure 1.4.

Reactive-near field approach

The method to be developed will use the elemental current distributions to estimate the reactance values of the varactors installed at their base. To achieve this, the reactive near magnetic (or electric) field distributions of the antenna elements will be measured. The current distributions can be derived from the reactive near fields. Once the current distribution on the ESPAR antenna elements are understood, the reactance values and radiation patterns can easily be calculated through a method described in [11].
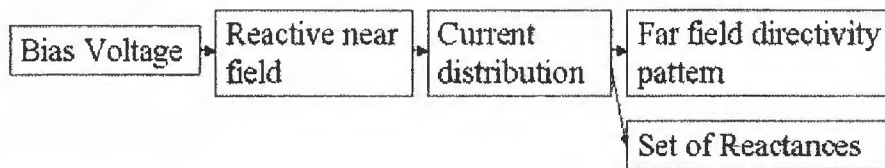
Figure 1.4: Story : Characterization of the ESPAR antenna

Chapter 2

Research Purpose and Background

2.1 The Purpose

Characterizing ESPAR antennae using conventional far field measurements in large anechoic chamber requires great effort and time. Therefore, reactive near field approach, that can be obtained with a small, inexpensive reactive near field anechoic box is a great improvement[7]. Simulation would highly help to prove this method. Moreover, finding a way of simulating the ESPAR antenna to compute both far field and reactive near field methods would decrease the time and efforts in comparison with experimental approach. Therefore, HFSS (High Frequency Structure Simulator), a smart software to design high frequency devices has been used during this internship to reach this goal.

2.2 Introduction to Equivalent Weight Vector approximation

2.2.1 Conventional Far Field approach

Rigorously speaking, antenna far field patterns are obtained by integrating electromagnetic components on a closed surface of an antenna[15],

$$\mathbf{E}(x, y, z) = \int_{S} (\langle j\omega\mu_0 \mathbf{H}_{tan}\rangle G + \langle \mathbf{E}_{tan} \times \nabla G \rangle + \langle \mathbf{E}_{normal} \nabla G \rangle) ds \quad (2.1)$$

where,

- $\mathbf{E}(x, y, z)$ represents the electric field external to the region bounded by a closed surface,

- s represents the radiation boundary surface,

- j is the imaginary unite, $\sqrt{-1}$,

- ω is the angular frequency, $2\pi f$,

- μ_0 is the relative permeability of the free space,

- $\mathbf{H}_{tan}$ is the component of the magnetic field that is tangential to the surface,

- $\mathbf{E}_{tan}$ is the component of the electric field that is tangential to the surface,

- $\mathbf{E}_{normal}$ is the component of the electric field that is normal to the surface,

- $\mathbf{G}$ is the free space Green's function, given by

$$G = \frac{e^{-jk_0|\mathbf{r}-\mathbf{r}'|}}{|\mathbf{r}-\mathbf{r}'|} \tag{2.2}$$

where,
  - k_0 is the free space wave number, $\omega\sqrt{\mu_0\epsilon_0}$,
  - $\mathbf{r}$ and $\mathbf{r}'$ represent, respectively, field points and source points on the surface.

In the far field where $r \gg r'$ (and usually $r \gg \lambda_0$), the Green's function can be approximated by

$$G \approx \frac{e^{-jk_0r}e^{jk_0\hat{r}\cdot\mathbf{r}'}}{r} \tag{2.3}$$

When this form of G is used in the far field calculations, the fields that result have an r dependence in the form of

$$\frac{e^{-jkr}}{r} \tag{2.4}$$

This r dependence is characteristic of a spherical wave, which is a key feature of far fields. The far field is a spherical TEM wave with the following equation

$$\mathbf{E} = \eta_0 \mathbf{H} \times \hat{\mathbf{r}} \tag{2.5}$$

where η_0 is the instrisic impedance of free space.

2.2.2   Reactive Near Field approach: the Equivalent Weight Vector approximation

The close surface where the current density is integrated belongs to the reactive near field, also known as the evanescent region[7]. It is evident that a great many points have to be measured from the reactive near field and computed to get a far field pattern by using equation (2.1). As a result, a far field analysis of even a small antenna would cost great time. Therefore, a method based on **Equivalent Weight Vector approximation (EWV)** in

which the far field patterns are calculated from the current only at discrete points is proposed. The far field directivity pattern of current-based antenna is calculated by using the following equations[4],

$$
\begin{aligned}
\mathbf{D}_a(\theta, \phi) &= \mathbf{i}^T \mathbf{a} \qquad\qquad (2.6) \\
\mathbf{i} &= [i_0, i_1, \ldots, i_n]^T, \\
\mathbf{a} &= [\mathbf{a}_0, \mathbf{a}_1, \ldots, \mathbf{a}_n]^T, \\
\mathbf{a}_k &= e^{j\beta \mathbf{r}_k^T \begin{bmatrix} \cos\theta\cos\phi \\ \cos\theta\sin\phi \\ \sin\theta \end{bmatrix}}
\end{aligned}
$$

where,

- $\mathbf{D}_a(\theta, \phi)$ represents the array factor,

- $\mathbf{i}$ equivalently plays the role of weight vector of the array antenna,

- $\mathbf{a}$ is the array' steering vector,

- $\mathbf{r}_k(k = 0, \ldots, n)$ is the position vector,

- θ is the elevation angle,

- and ϕ is the azimuth angle (cf. Figure 2.1).
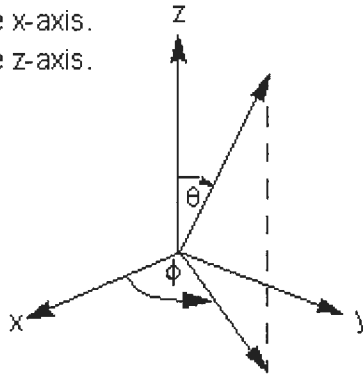
Figure 2.1: Spherical coordinates

It is clear that the antenna's directivity can be easily understood as long as the antenna element currents are offered since the other parameters in (2.6) are constants.

2.3 Experimental Scheme and Results

2.3.1 Experimental Setup

Experiments has been led by Dr. Han in order to investigate the reactive near field method[4, 7, 9]. The experimental scheme used is shown in Figure 2.2.
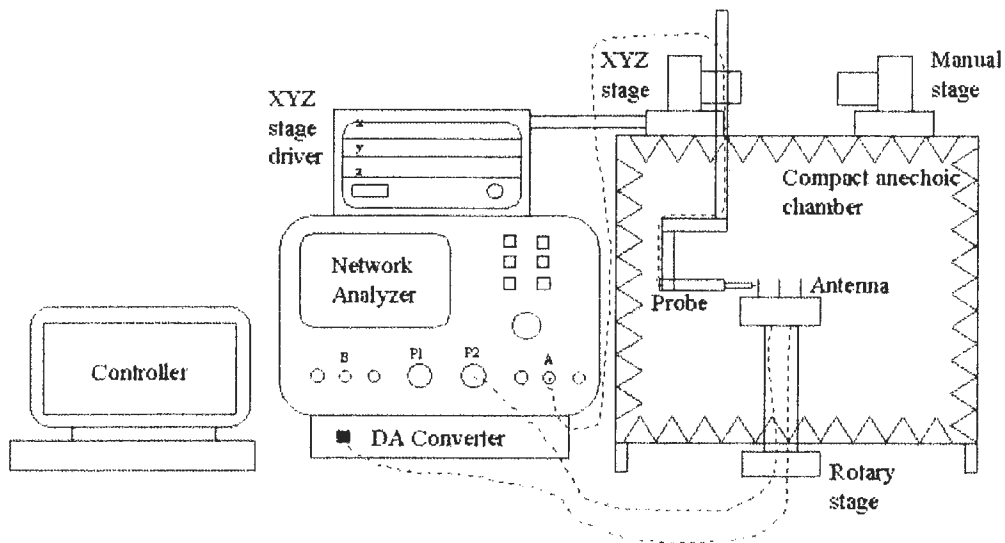
Figure 2.2: Experimental Scheme

A Digital to Analog Converter (DAC), linked to a PC, supplies the control voltages so that the individual varactors could be set to obtain the desired beam and nulls for the directivity patterns.

As the ESPAR antenna is a small, low cost antenna, it would be unfortunate to invest in a large anechoic chamber. Setup and maintenance expenses coupled with impractical measurement configurations make it desirable to use a small, inexpensive anechoic box instead. Therefore, studies and experiments have been led to ascertain the minimum size of the Reactive Field Anechoic Box (RFAB) used for these experiments so that only the measurement probes are inside the box[4, 7, 9]. The actual size of the designed RFAB is about $60 \times 60 \times 60$ cm^3, with its internal size equals to 3λ with $\lambda = 12.08$ cm ($f = 2.484Ghz$).

Eventually, a Network Analyzer, positioned outside the RFAB, measures the RF signals probed in the reactive near field of the antenna.

2.3.2 Measurement Results

The EWV results obtained through a derivation of equation (2.6) are depicted in Figure 2.3 with solid lines. The dotted lines show the measured far field patterns using the conventional method. Both omni and beam patterns show good agreements between the reactive near field measurement method and the direct far field pattern measurement method.
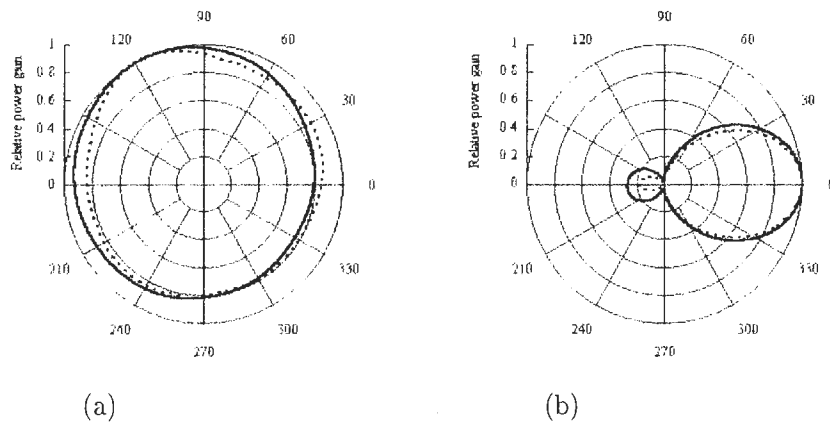
Figure 2.3: Experimental far field power patterns (a) when controlled to omni directional. (b) when beamformed in the direction of 0°.

Eventually, the method that uses the measured elemental reactive near electromagnetic fields of a small antenna to obtain its far field pattern is shown to be valid.

Chapter 3

HFSS Simulation of Conventional Far Field and Reactive Near Field Methods

3.1   Introduction to HFSS

Introduced in 1990, Ansoft HFSS is an interactive software package for calculating the electro-magnetic behavior of a structure[14]. Based on the concept of Finite Element Method (FEM - see below), the software automatically computes multiple adaptative solutions until a user-defined convergence criterion is met. Field solution calculated from first principles predict all high-frequency behavior such as losses due to materials and radiation.

An initial mesh - or subdivision of the geometry into tetrahedral elements - is created based on the structure drawn in the Computer-Aided Drawing (CAD) package. This initial mesh will solve to provide field solution information identifying regions of high field intensity or rapid field gradients. The mesh is then refined only where needed, saving computational resources while maximizing accuracy. If desired, the user can guide the adaptive solution using a manual meshing interface.

Eventually, HFSS includes post-processing commands for analyzing the electro-magnetic behavior of the structure in more detail: basic electro-magnetic quantities (electric field E, magnetic field H, volume current J) and, for open boundaries problems, radiated near and far fields, characteristic port impedances, propagation constants, and S-parameters[2].

3.2   Simulated ESPAR structure

The design of the antenna to simulate is in Figure 3.1.

The frequency is $f = 2.484GHz$, that is to say the wavelength equals $\lambda = 120.8mm$.
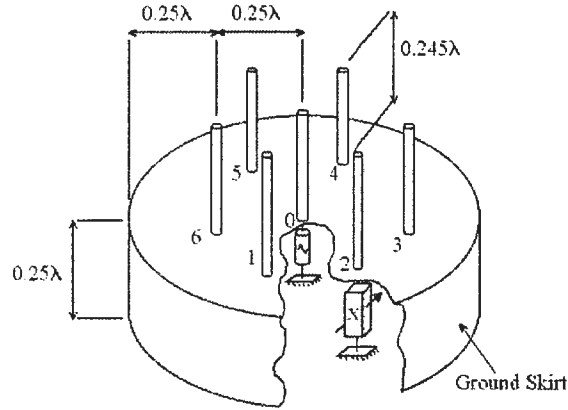
Figure 3.1: ESPAR antenna structure

3.2.1 3D Model

The ground skirt is modeled with a cylinder without any bottom. The radius and height of the skirt are $\frac{\lambda}{2} = 60.4mm$ and $\frac{\lambda}{4} = 30.2mm$, respectively. Then, the elements are designed using cylinders which radius and height are 1mm and 29.6mm[1], respectively. A radiation boundary is defined to limit the volume where the software has to compute the mesh. The size of this boundary has to lay between $\frac{\lambda}{3}$ and λ. Therefore, we used a cylinder which radius and height are 100mm and 140mm, respectively, that is to say around $\frac{\lambda}{4}$. Figure 3.2 shows how the model has been drawn using HFSS.

As the method to design the ESPAR antenna structure is long, the steps are described in Appendix 1.

Note: The model used is based on "Lumped RLC" Boundary to simulate the Reactances of the ESPAR antenna. In order to get the values of the set of reactances, which are Capacitance values in our model, the function "Capa.m", available in Appendix 6, converts a Bias voltage value ($V\epsilon[-2048V, 2047V]$) or a Reactance value ($X\epsilon[-4.7\Omega, -93.7\Omega]$) into the wanted Capacitance value ($C\epsilon[1.3e^{-11}F, 6.9e^{-13}F]$).

3.2.2 Finite Element Method

In HFSS, the geometric model is automatically divided into a large number of tetrahedra, where a single tetrahedron is basically a four-sided pyramid (cf. Figure 3.3). This collection of tetrahedra is referred to as a *finite element mesh*. Figure 3.4 shows the mesh that was created for the ground skirt of our ESPAR antenna structure.

---

[1]The element height is slightly shorter than $\frac{\lambda}{4}$.
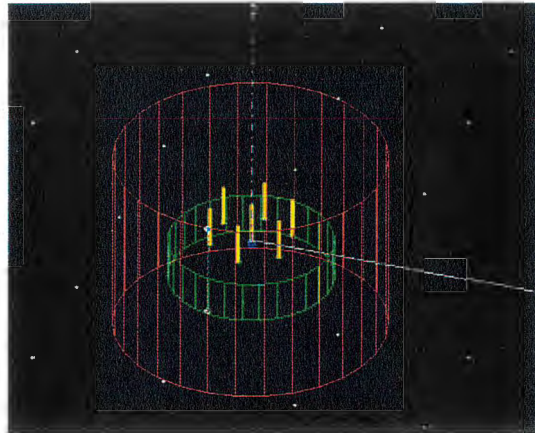
Figure 3.2: ESPAR antenna structure designed using HFSS
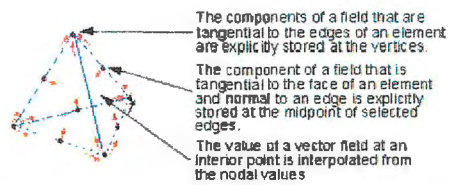
Figure 3.3: Tetrahedra Definition in HFSS
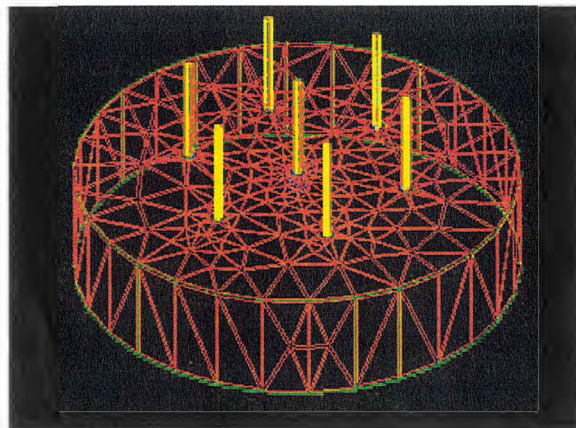
Figure 3.4: Ground Skirt Resulting Mesh

Dividing a structure into thousands of smaller regions (elements) allows the system to compute the field solution separately in each element. The

smaller the system makes the elements, the more accurate the final solution will be.

Note: The details on how to refine a mesh created on the ESPAR model in order to get more accurate results are explained in Appendix 2. This refinement has been very helpful to get precise far field directivity patterns. Indeed, without any refinement, the number of tetrahedra used to compute the structure was not important enough, and then, for an ideal case as Omni pattern which is supposed to perfectly symmetrical the pattern obtained was not circular!

3.3 Simulation Methods and Results

Once a solution as been generated, the analyze is possible using HFSS' post-processing features, accessed with the **Post Process** menu.

Firstly, the far field plot is computed, on the basis of the conventional far field approach described in section 3.2.1 of Chapter 3. The steps on how to get this pattern are described in Appendix 2. The resulting pattern file has the format *.dat*.

Secondly, the current values are calculated on discrete points picked up on the HFSS antenna structure. The 3D Post Process Calculator is used to get these values. The use of this Calculator is described in more details in Appendix 2. The resulting files containing the values of the currents have the format *.reg*.

Then, these current values are used in the Equivalent Weight Vector approximation described in section 3.2.2 of Chapter 3. The EWV approximation resulting pattern values are computed using Matlab software. The Matlab code sources are available in Appendix 4 and 5. The main program is "CompSimExp.m". Its input files are the directivity pattern data *.dat* and current data *.reg*. It uses the function "CrossCorrel.m" to calculate the cross correlation coefficient between the two patterns computed. Every step is explained in more details in Appendix 2.

The results of the far field and reactive near field approaches are shown in Figure 3.5 and 3.6.

Omni pattern results

An omni pattern is supposed to be as circular as possible as the antenna should radiate the same field intensity in every direction if the structure is perfectly symmetrical. Firstly, simulation has been led for Omni pattern, that is to say where all reactances values are equals. In our case, we used a $(x_1, x_2, \ldots, x_6) = (-90\Omega, -90\Omega, \ldots, -90\Omega)$ set of reactances[2]. A perfect

---

[2]The values are in Ω. The real values used for the simulation are in Farad, converted by the program *Capa.m*.

circle has been obtained after refinement[3], corroborating the fact that the simulation tends to stick to reality. Indeed, simulation is supposed to be the ideal case describing the real behavior of the device. In Figure 3.5, the solid and dotted lines represent the far field and EWV approximation resulting patterns respectively, for this omni pattern.
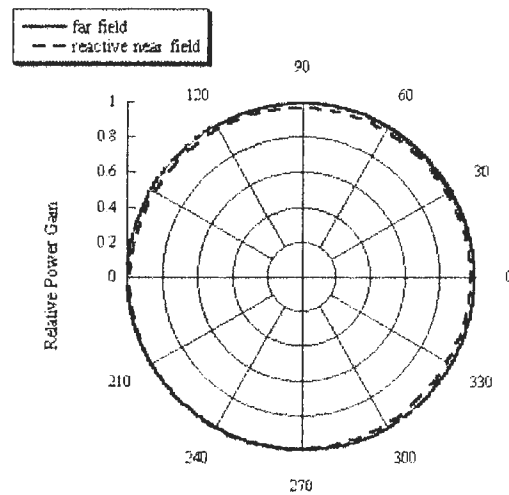
Figure 3.5: Simulation Results for Omni pattern

---

[3]See Appendix 2 for Refinement explanations.

(a)

(b)

(c)

(d)

(e)

(f)

(g)
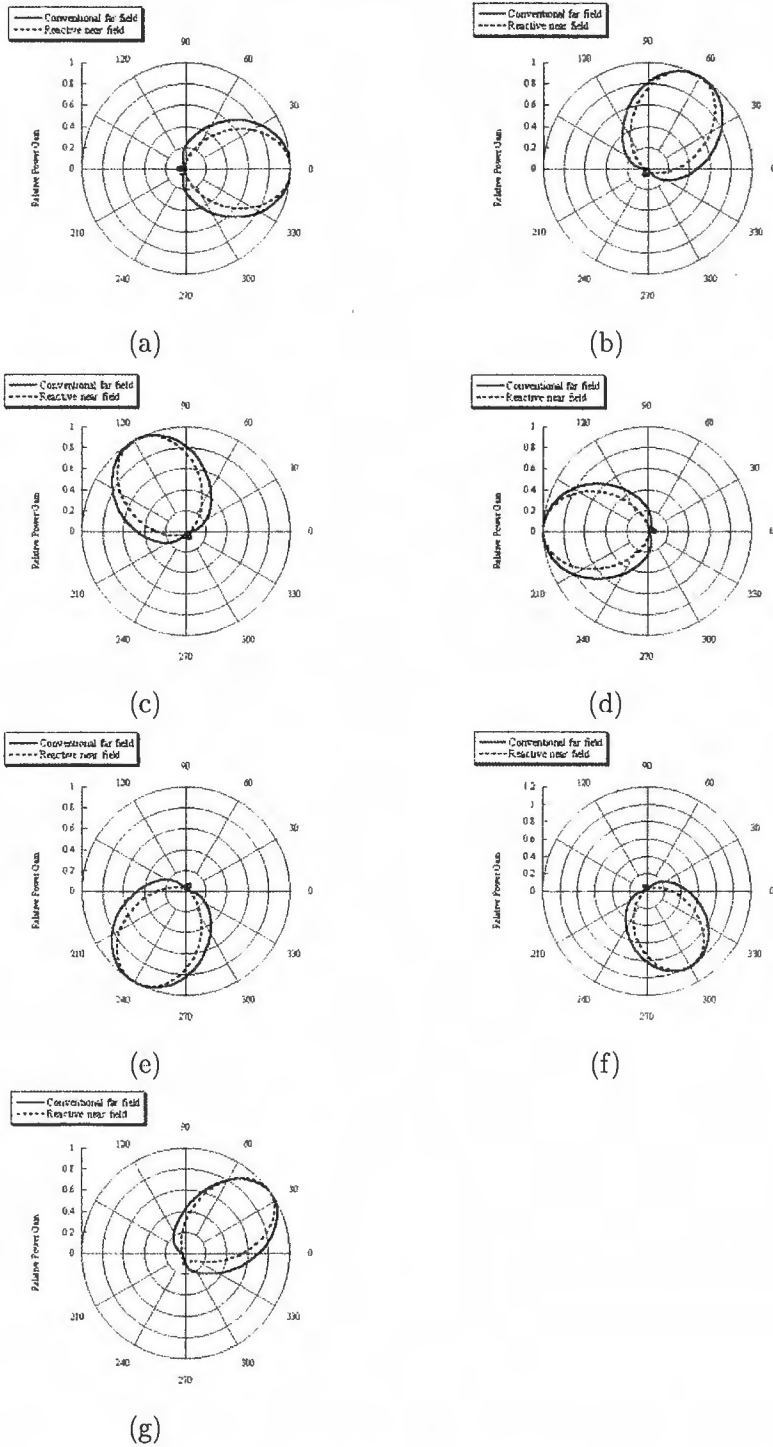
Figure 3.6: Simulation Results for Beam patterns when 1 point per element is picked up (a) 0°-Beam. (b) 60°-Beam. (c) 120°-Beam. (d) 180°-Beam. (e) 240°-Beam. (f) 300°-Beam. (g) 30°-Beam.

Beam pattern results

Secondly, simulation has been done for Beam patterns for Direction Of Arrivals (DoA) of 0°, 30°, 60°, and multiples of 60° as 120°, 180°, 240°, and 300°. Beam patterns are supposed to have their maximum radiation intensity in the chosen direction. In our case, the set of reactances used, wich had been obtained by experimental beamforming[4], are shown in table 3.1. The 60° multiples DoA have all been simulated, whereas only 30° has been simulated for the 30° multiple DoA. In Figure 3.6, the solid and dotted lines represent the far field and EWV approximation resulting patterns respectively, for each of these DoA. Far field patterns obtained by conventional far field method using HFSS actually have their maximum directivity gain in the wanted direction. For instance, the 0° beam pattern has his maximum gain at 0°. This tends to prove that the structure designed using HFSS is sufficiently accurate to simulate the real -experimental- structure.

Table 3.1: Set of Reactances used in Simulations: $(x_1, x_2, \ldots, x_6)$

Omni	$(-90\Omega, -90\Omega, -90\Omega, -90\Omega, -90\Omega, -90\Omega)$
0°	$(-90\Omega, 0\Omega, 0\Omega, 0\Omega, 0\Omega, 0\Omega)$
30°	$(-92.0458\Omega, -92.3930\Omega, -4.7684\Omega, -12.9059\Omega, -16.1609\Omega, -4.7684\Omega)$
60°	$(0\Omega, -90\Omega, 0\Omega, 0\Omega, 0\Omega, 0\Omega)$
120°	$(0\Omega, 0\Omega, -90\Omega, 0\Omega, 0\Omega, 0\Omega)$
180°	$(0\Omega, 0\Omega, 0\Omega, -90\Omega, 0\Omega, 0\Omega)$
240°	$(0\Omega, 0\Omega, 0\Omega, 0\Omega, -90\Omega, 0\Omega)$
300°	$(0\Omega, 0\Omega, 0\Omega, 0\Omega, 0\Omega, -90\Omega)$

Nevertheless, it appears that the EWV approximation results obtained for the beam patterns do not show as good agreements as for the omni pattern. Indeed, the conventional far field pattern and the pattern obtained by approximation are not that close one to the other. Therefore, the EWV approximation has been calculated for more than one current value per element. Figure 3.7 shows the patterns obtained when 5 points per element are picked up, and Figure 3.8 shows the patterns obtained by the EWV approximation method for 1, 5, 10, 20 and 40 points per element, respectively (cf. Figure 3.9), in the DoA of 60°. **Obviously, the more points picked up are, the better the approximation is.**

---

[4]The values used had been studied in the following paper: [13]

(a)

(b)

(c)

(d)

(e)

(f)

(g)
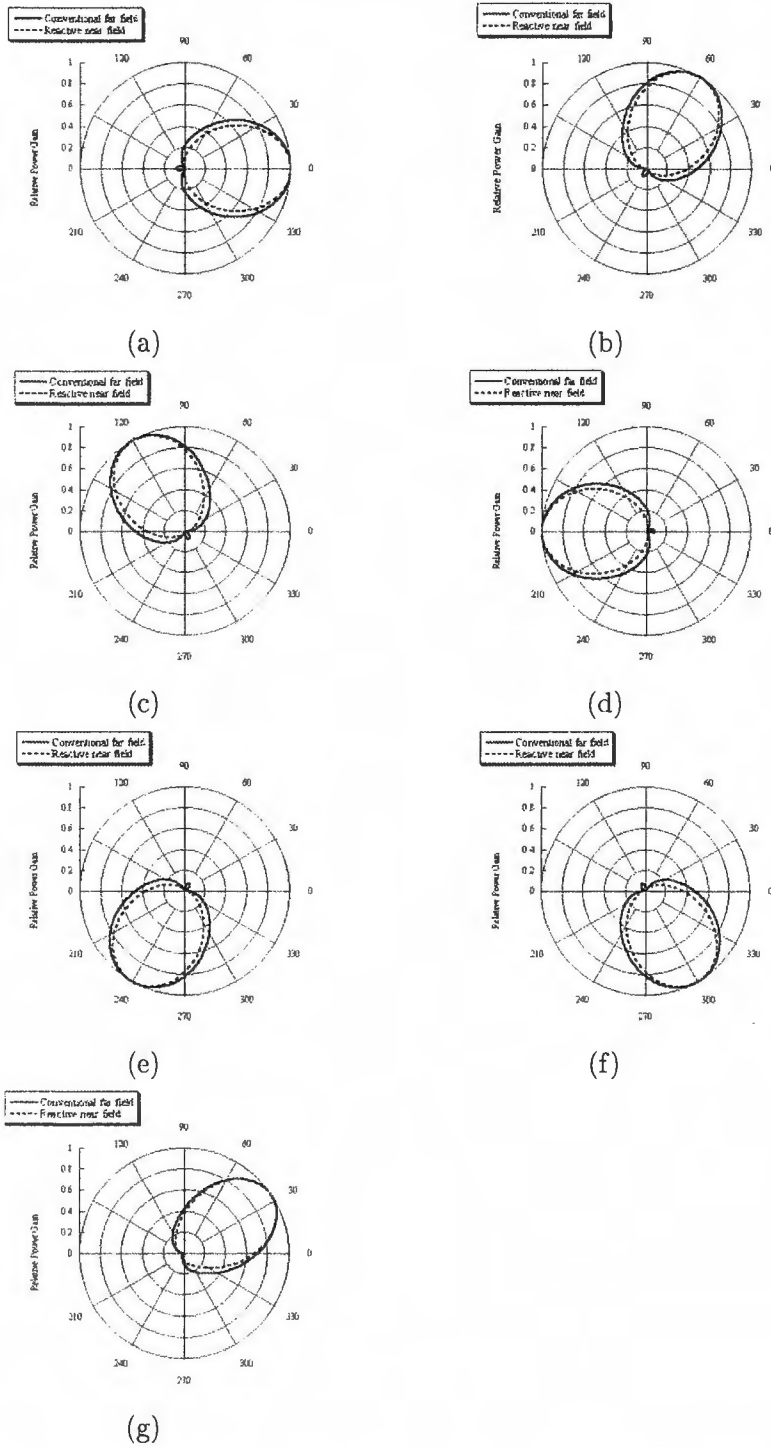
Figure 3.7: Simulation Results for Beam patterns when 5 points per element is picked up (a) 0°-Beam. (b) 60°-Beam. (c) 120°-Beam. (d) 180°-Beam. (c) 240°-Beam. (f) 300°-Beam. (g) 30°-Bcam.

(a)

(b)

(c)

(d)

(e)
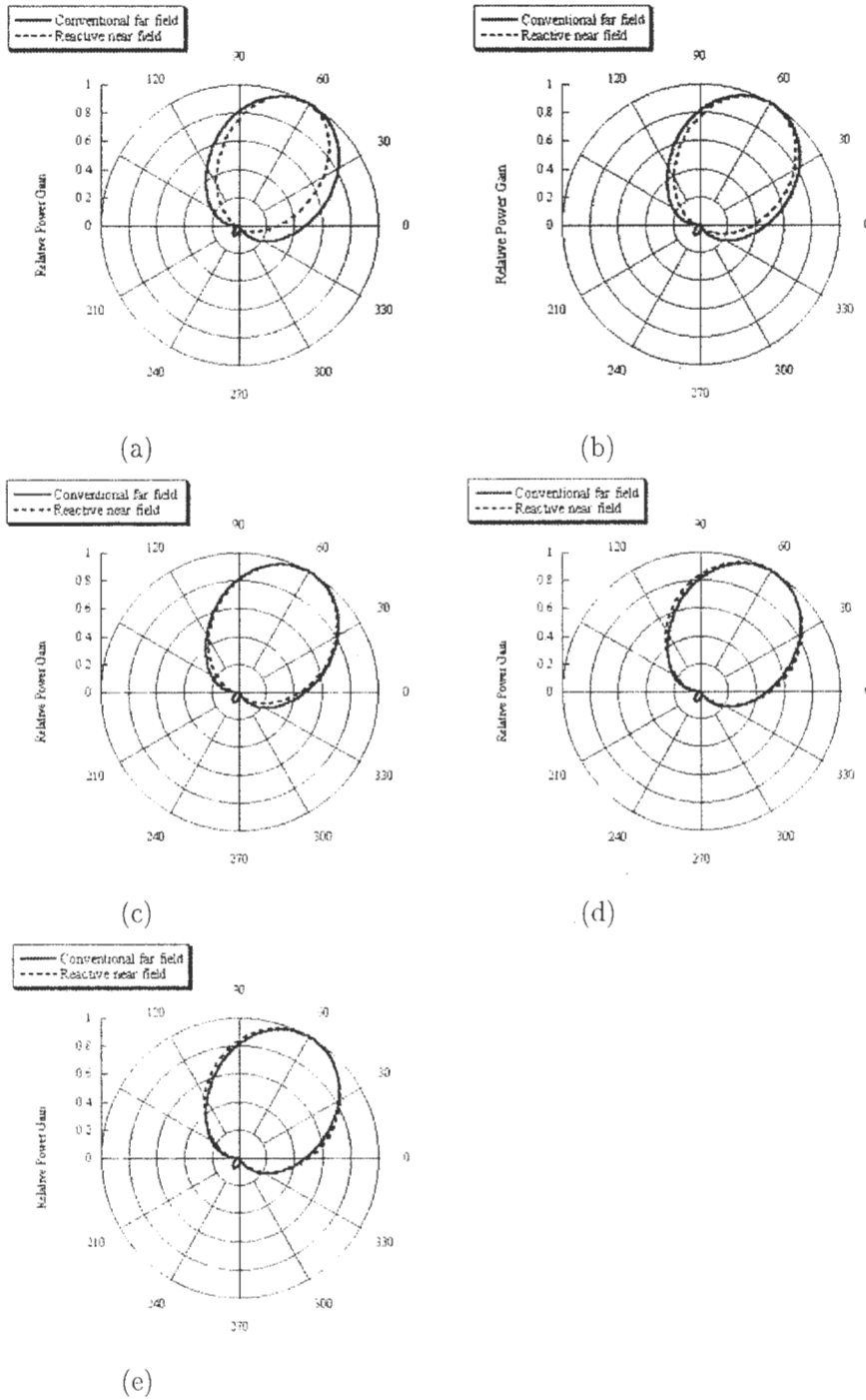
Figure 3.8: Simulation Results for 60°-Beam patterns (a) when 1 point per element is picked up. (b) when 5 points per element is picked up. (c) when 10 points per element is picked up. (d) when 20 points per element is picked up. (e) when 40 points per element is picked up.
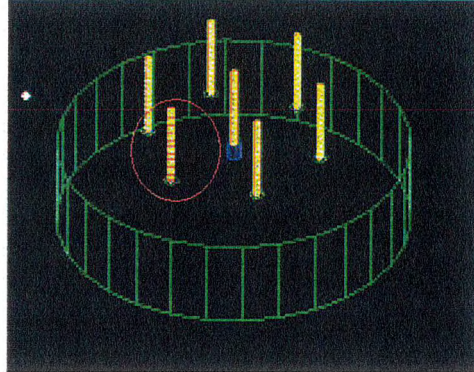
Figure 3.9: Points Picked Up per element on the ESPAR antenna structure

Quantification of the results

In order to quantify the difference between two patterns, we introduce the cross correlation coefficient, calculated as in equation 3.1

$$\rho = \frac{\oint \mathbf{D}_a(\theta, \phi)\mathbf{D}_f(\theta, \phi)^\star d\theta d\phi}{\sqrt{\oint \mathbf{D}_a(\theta, \phi)^2 d\theta d\phi}\sqrt{\oint \mathbf{D}_f(\theta, \phi)^2 d\theta d\phi}} \tag{3.1}$$

where, $\mathbf{D}_a(\theta, \phi)$ represents the array factor, as described in equation 2.6, and $\mathbf{D}_f(\theta, \phi)$ is the far field pattern. The superscript* means a complex conjugate. The value of ρ falls in $0 \leq |\rho| \leq 1$

Table 3.2 shows cross correlation coefficients between simulated conventional far field method and simulated EWV approximation.

Interpretation of the Results

The EWV approximation applied to the omni pattern shows good results, with a cross correlation coefficient of 0.999936 between this approximation method and the conventional one.

For the beam patterns, EWV approximation does not show that good agreements when only one point - current value - per element is picked up. Indeed, the cross correlation coefficients range from 0.979207 to 0.983698 between conventional far field and reactive near field approaches for the different beam directions. However, when more than one current value per element is used to calculate the far field pattern with the EWV approximation, the cross correlation coefficients become higher. These cross correlation coefficients are shown in table 3.2, and the graph 3.10 shows the evolution of these coefficients versus this number of points per element.

3.3. *SIMULATION METHODS AND RESULTS* Table 3.2: Cross correlation coefficients between far and reactive near field simulated approaches versus the number of points per element used to calculate the EWV approximation

Points	Omni	Beam:Angles of desired signal						
		0°	30°	60°	120°	180°	240°	300°
1	0.999936	0.979597	0.979207	0.983698	0.983285	0.980582	0.980999	0.980458
5	0.999961	0.992015	0.996352	0.993508	0.992187	0.99249	0.992653	0.992037
10	0.999979	0.996509	0.998143	0.996961	0.996427	0.996836	0.996908	0.996502
20	0.999979	0.998186	0.99895	0.998099	0.998261	0.998296	0.998331	0.99827
30	0.99998	0.99809	0.998799	0.998058	0.99814	0.998204	0.998215	0.998122
40	0.99998	0.998197	0.998888	0.998106	0.998265	0.998307	0.998332	0.998277

Eventually, the optimum value for the number of points picked up per element can be deduced from this graph 3.10 where the cross correlation coefficient is converging towards the stationary value 0.997548. Indeed, from the x-coordinate value of 10 (e.g. 10 points are picked up per element), the cross correlation coefficient does not evoluate much, which means that the approximation can be better, but provided that much efforts and time are spent for this small improvement. Using a 0.1% rule[5], as it is shown with a red line is on graph 3.10, we finally find that picking up 10 points per element to compute the EWV approximation is the optimum choice.
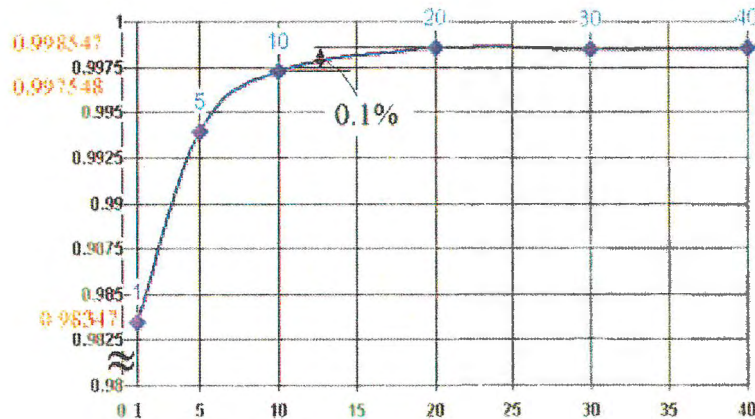
Figure 3.10: Cross correlation coefficients Vs. number of point per element used for the EWV calculation

---

[5]We calculate the number of point which correspond to 0.1% lower than the 0.998547 convergence value: 0.9975479535

3.4 Comparison between Simulation and Experiments

Once the simulation has been achieved, showing that the EWV approximation can be used to get far field pattern more easily, a comparison can be set up between those simulated results and the experimental ones.

Firstly, the conventional far field methods are compared, as it is shown in Figure 3.11 and 3.12. The solid and dotted lines represent the simulated and experimental far field patterns respectively.
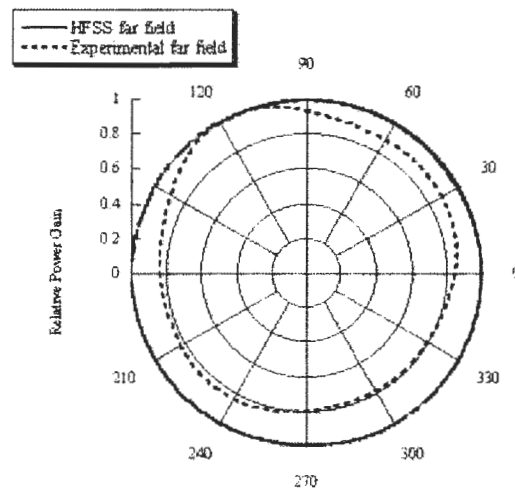
Figure 3.11: Experimental and Simulated far field omni patterns obtained by conventional approach

The general shape of the curves are similar, even if the experimental omni pattern is not as a perfect circle as the simulated one, due to experiments imperfections. The shape of the beams are close one to the other, the 0° direction being faithfully obtained.

Secondly, experimental and simulated reactive near field results are compared to conventional far field method. Figure 3.13 shows that, in the omni case, because the simulated and experimental conventional method patterns were different from the beginning, the approximated method patterns cannot be compared properly. Indeed, the reactive near field approach patterns for both experiments and simulations are close to their respective conventional far field method pattern, but very different one to the other.

On an other hand, Figure 3.14 shows that, in the 0°-Beam case, whereas the simulated reactive near field and far field methods patterns were not that close, the EWV approximation simulated results yield a similar far field

Figure 3.12: Experimental and Simulated far field 0°-beam patterns obtained by conventional approach

pattern to the experimental conventional one. This last result implies that Simulation can be used to predict a beamformed far field pattern from the values of a set of reactances.
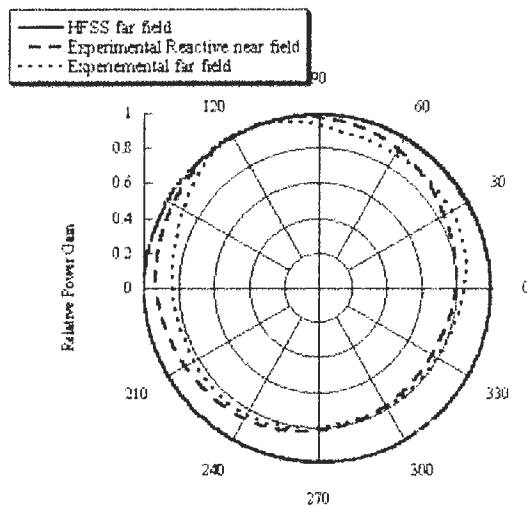
Figure 3.13: Omni case: Reactive near field and far field Experimental patterns Vs. Simulated far field pattern
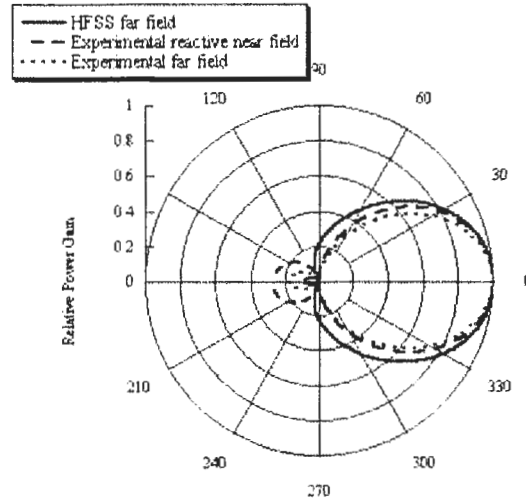
Figure 3.14: 0°-Beam case: Reactive near field and far field Experimental patterns Vs. Simulated far field pattern

Other simulations has been led with other sets of reactances which have also been tested during experiments (See Values used in [13]). As a conclusion, it appears that each experimental set of reactance yields experimental far field patterns and simulated patterns which show good agreements one to the other.

3.5 Conclusion on these Results

Eventually, simulation has been proved to yield good results using the antenna design described in Section 4.2.1 of this Chapter. Indeed, the directivity far field patterns obtained by simulation were similar to the one obtained by experiments. The optimum number of points to be picked up on the antenna is 10, when those points are picked up on the elements. But, research has to be continued to study if this number decrease when points are picked up on the ground surface, and not only on the elements. Furthermore, when simulating beamformings, it appears that the results shows good agreements with the experimental ones, which implies that HFSS Simulator can be used in the future to predict beamforming in an easier way than the experimental one. Future research will be led on using Genetic Algorithms in order to find by simulation the optimum set of reactances that implies specific and accurate beamformings.

Note: 3D radiation directivity pattern can be computed with HFSS, as shown in Figure 3.15.
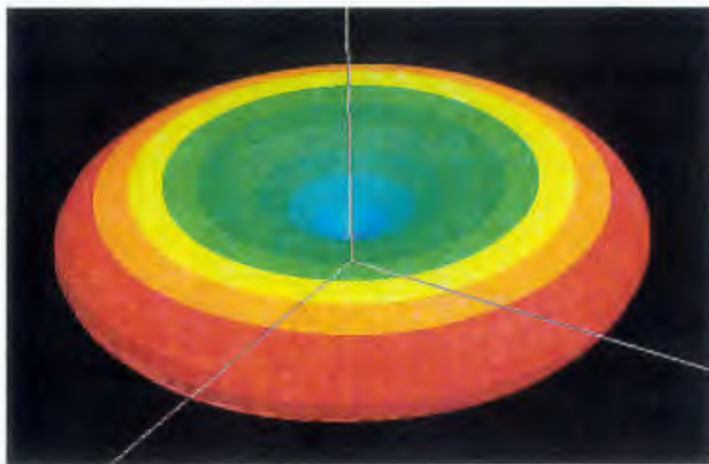
(a)
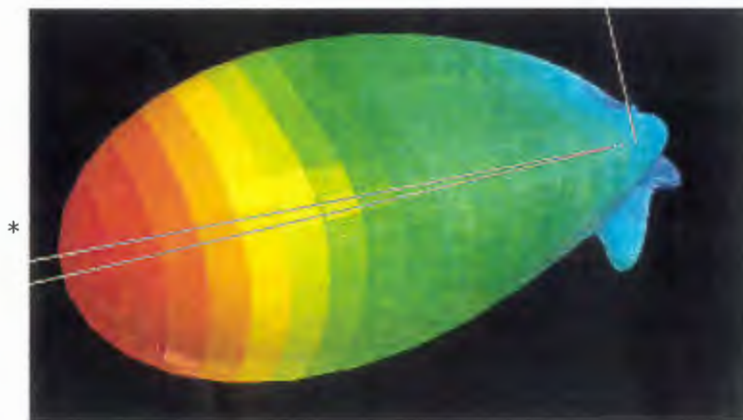
(b)

Figure 3.15: 3D Far field power patterns (a) when controlled to omni directional. (b) when beamformed in the direction of 0°.

CONCLUSION

This paper proposes a way of simulating the ESPAR antenna using HFSS software. Its flexibility comparing to the usual experimental techniques when getting a radiation pattern from a precise set of reactances brings a great improvement in efforts and time spent. A reactive near field approach based on Equivalent Weight Vector approximation has been studied. This approximation can be used to obtain far field patterns in order to characterize the antenna. An optimum number of data needed to use this approximation has been found, which implies that EWV approximation can be used efficiently in the future. This work on Simulation may have an important effect on future researches in ACR-Dept. 3, as it can be used to study the antenna optimization, which is still a hot topic. Further research will be to use Genetics Algorithms in order to find optimum sets of reactances for beamforming.

Bibliography

[1] Microwave Terminology webpage, http://www.cccosorb.com/terminology.asp, May 2002.

[2] Scattering Parameters webpage, http://www.ee.surrey.ac.uk/Personal/D.Jefferies/sparam.html, May 2002.

[3] ATR-ACR webpage, http://www.acr.atr.co.jp , August 2002.

[4] T. Ohira, K. Gyoda, A. Akiyama, and K. Yang, "Equivalent Weight Vector and Array Factor Formulation for ESPAR antennas," IEICE Technical Report, AP2000-44, SAT2000-41, NW2000-41, July 2000.

[5] R. Schlub, J. Lu and T. Ohira, "Frequency Response of the ESPAR Antenna: Numerical Estimation by Methods of Moments, Finite ELements, and FDTD," IEICE Technical Report, AP2001-2, April 2001.

[6] J. Cheng, Y. Kamiya and T. Ohira, "Adaptive Beamforming of ESPAR Antenna Based on Steepest Gradient Algorithm," IEICE Trans. Commun., vol. E84-B, no. 7, pp. 1790–1800, July 2001.

[7] Q. Han, K. Inagaki , K. Iigusa , R. Schlub and T. Ohira, "Reactive-Field Anechoic Box for ESPAR Antenna Measurement," IEICE Trans. Commun., vol. E85-C, no. 7, pp. 1451–1459, July 2002.

[8] S. Tawara, K. Gyoda, T. Ohira, Y. Ojiro, S. Saito amd H. Kawakami, "Beam Steering Experiments of 7 Elements of ESPAR Antenna by Using Monte Carlo Method," Proc. of the 2000 commu. society conf. of IEICE, B-1-117, September 2000.

[9] Q. Han, K. Inagaki , K. Iigusa and T. Ohira, "Development of Compact Anechoic Box - Antenna RF Measurement Based on a Reactive-Near-Field-Probing Technique," IEICE Trans. Commun.,A-P2002-17, SAT2002-7, May 2002.

[11] T. Ohira and K. Gyoda, "Hand-held Microwave Direction-of-Arrival Finder Based on Varactor-Tuned Analog Aerial Beamforming," Proc. of APMC2001, Vol. 2 of 3, pp. 585-588, December 2001.

47

[12] E. Taillefer, "Implementation of Adaptive Controller for ESPAR Antenna by Using DSP and Experiments for Performance Verification," Advanced Telecommunications Research Laboratories, 2001.

[13] K. Iigusa, M. Hashiguchi, A. Hirata and T. Ohira, "ESPAR Antenna Parameters Fitting Based on Measured Data," IEICE Technical Report, AP2001-104, RCS2001-143, October 2001.

[14] HFSS v8.5 Developed by Ansoft Corp.. Further information is available at http://www.ansoft.com, August 2002.

[15] Maxwell On-Line Help, HFSS v8.5 Developed by Ansoft Corp.. August 2002.

[16] Ansoft Corp.., "Ansoft HFSS - Getting Started: An Antenna Problem," Ansoft HFSS v7.0 October 1999.

[17] Ansoft Corp.., "Ansoft HFSS - Introduction to the Ansoft Macro Language," Ansoft HFSS v8.5 March 2002.

[18] J. Guivarc'h and M. Guyomard, "Presentation d'un Rapport Scientifique et Technique - Structure - Typographie - Langue - Recommandations," École Nationale Supérieure de Sciences Appliquées et de Technologie, February 1994.

[19] Leslie Lamport, "LATEX, User's Guide & Reference Manual,"Addison-Weshley Publishing Company, 1986, ISBN 0-201-15790-X.

APPENDIX 1: PROCEDURE FOR SIMULATING THE ESPAR ANTENNA IN HFSS
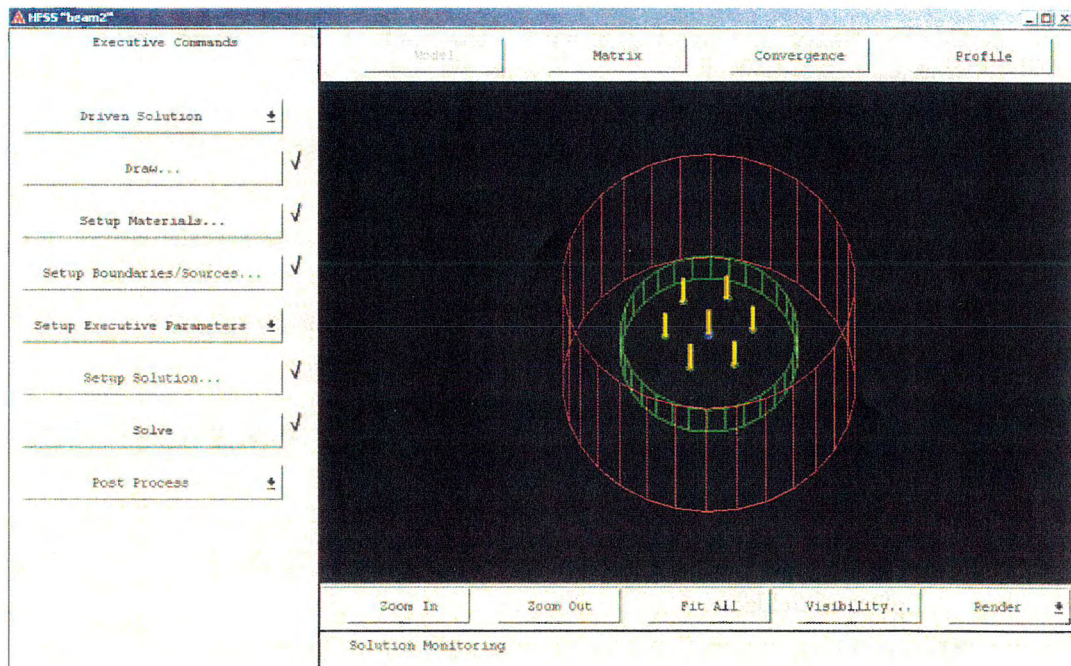
Figure 1.16: HFSS Main Project Window

General Procedure for Drawing and Solving

Here are the steps to follow when defining and solving a problem using HFSS.

1. Use the **Draw** command to access the 3D Modeler and draw the objects that make up the geometric model.

49

2. Use the **Setup Materials** command to assign material characteristics to each 3D object in the geometric model.

3. Use the **Setup Boundaries/Sources** command to define the location of the boundaries and sources.

4. Use the **Setup Solution** command to specify how the solution to the problem is to be computed. Use this command to:

   - Select the type of solution to be performed - an adaptative analysis or a frequency sweep.
   - Enter solution criteria, such as the frequency (or frequency range for a sweep), port solution accuracy, and so forth.
   - Select which finite element mesh is used for the solution.

5. Use the **Solve** command to solve for the fields associated with the antenna problem.

6. Use the **Matrix**, **Convergence**, and **Profile** buttons to view the following information:

   - The S-parameters, impedances, and propagation constants computed during each adaptative solution.
   - The difference in S-parameters between each adaptative solution.
   - Statistics on CPU use, memory size, and so forth.

7. Select one of the following Post Processors from the **Post Process** menu:

   Fields Accesses the 3D Post Processor which allows you to display contour, shaded, vector, values versus distance, and animated plots of fields.

   Matrix Data Accesses the Matrix Data Post Processor which allows you to view matrices computed for the S-parameters, impedances, and propagation constants during each adaptative solution.

   Matrix Plot Accesses the Matrix Plot Post Processor which allows you to plot variety of parameters versus time or frequency.

Figure 1.16 shows the commands previously described. They must be chosen in the sequence in which they appear. For example, you must create a geometric model with **Draw** before you specify material characteristics for objects with **Setup Materials**. A checkmark appears on the menu next to each step as it is completed.

ESPAR Model

Here is the step by step procedure for making an ESPAR antenna that works in HFSS. Before attempting to do this, I suggest you try the HFSS tutorial given in the manuals so you knowledge on how to do the basic functions.

Steps:

1. **Create a project**

2. **Draw...**

   Select "Draw..." from the Main menu

   (a) A warning screen about units comes up. Read it as it has important information, choose unit "mm" and click OK.

   (b) **First we draw the ground plane**

      i. Coordinate Field: set $x = 0$, $y = 0$, $z = 0$.
      ii. MenuBar → Lines → Circle
      iii. LeftField
         - Circle Axis: Z
         - Circle Center: Enter button
         - Radius: 60.4 *% Radius of Ground plane*
         - Num segments: 30 *% Number of circle sides*
         - Name: Ground
         - Color: click on the gray box and select Green
         - Enter Button
      iv. Zoom in over the crossing between "Ground" circle and X axis so that you could see at least a full segment.

   (c) **Next we will create a rectangle on one of the sides of the "Ground" circle and then copy and paste it to every side to make a ground skirt.**

      i. Menu → Lines → PoyLine
      ii. LeftField:
         - Edit
           Create: GroundSkirt
         - OK Button
         - Color: Click on the gray box and select Green
      iii. Use the mouse to click on vertex of "Ground" circle that crosses with the X axis (at point $(60.4; 0; 0)$).
      iv. LeftField:
         - Enter Button *% A little cross should appear on the point in the drawing*

v. Use the mouse to click on neighbouring vertex (of the one you just clicked on - should be at $(59.0801\ldots; 12.5578\ldots; 0)$)

vi. LeftField:

- Enter Button

vii. COORDINATES: $z = -30.2$ *% Depth of the Ground Skirt*

viii. LeftField:

- Enter Button

ix. COORDINATES: $x = 60.4$, $y = 0$.

x. LeftField:

- Enter Button
- Close Button
- Done Button

xi. SELECT "GroundSkirt"

xii. COPY

xiii. PASTE

xiv. ROTATE Axis Z Angle 12.

xv. UNITE "GroundSkirt" "GroundSkirt1"

xvi. SELECT "GroundSkirt"

xvii. COPY

xviii. PASTE

xix. ROTATE Axis Z Angle 24.

xx. UNITE "GroundSkirt" "GroundSkirt1"

xxi. SELECT "GroundSkirt"

xxii. COPY

xxiii. PASTE

xxiv. ROTATE Axis Z Angle 48.

xxv. UNITE "GroundSkirt" "GroundSkirt1"

xxvi. SELECT "GroundSkirt"

xxvii. COPY

xxviii. PASTE

xxix. ROTATE Axis Z Angle 96.

xxx. UNITE "GroundSkirt" "GroundSkirt1"

xxxi. SELECT "GroundSkirt"

xxxii. COPY

xxxiii. PASTE

xxxiv. ROTATE Axis Z Angle 168.

xxxv. UNITE "Ground" "GroundSkirt" "GroundSkirt1"

(d) **We now have a complete ground plane skirted along its border. Time to make the monopoles and impedance pads.**

i. COORDINATE: $x = 0$ $y = 0$ $z = 0$

ii. CIRCLE Axis:Z Radius:2.31 Segments:12 Name:Pad Color:Peach

iii. COORDINATE: $x = 0$ $y = 0$ $z = 0$

iv. CYLINDER Axis:Z Radius:1 Height:29.6 Segments:12 Name:Element Color:Yellow

v. SELECT "Element" "Pad"

vi. ROTATE 15 degres axis:Z

vii. COPY

viii. PASTE

ix. SELECT "Element1" "Pad1"

x. MOVE $x = 30.2$

xi. RECTANGLE First Point: $x = 27.968711341272252257608093208626$ % x=30.2-2.31*cos(15°)
$y = -0.2588190451025207623488988376240 5$ % y=-sin(15°)
$z = 0$
Rectangle Plane: XY
Size: $x = 1.2653628324386794556421635916449$ % x=1.31*cos(15°)
$y = 0.517638090205041524697797675248 1$ % y=2*sin(15°)
Name:Imped1 Color: Blue

xii. SELECT "Element1" "Pad1" "Imped1"

xiii. COPY

xiv. PASTE

xv. PASTE

xvi. PASTE

xvii. PASTE

xviii. PASTE

xix. SELECT "Element2" "Element3" "Element4" "Element5" "Element6" "Pad2" "Pad3" "Pad4" "Pad5" "Pad6" "Imped2" "Imped3" "Imped4" "Imped5" "Imped6"

xx. ROTATE Axis:Z Angle:60

xxi. SELECT "Element3" "Element4" "Element5" "Element6" "Pad3" "Pad4" "Pad5" "Pad6" "Imped3" "Imped4" "Imped5" "Imped6"

xxii. ROTATE Axis:Z Angle:60

xxiii. SELECT "Element4" "Element5" "Element6" "Pad4" "Pad5" "Pad6" "Imped4" "Imped5" "Imped6"

xxiv. ROTATE Axis:Z Angle:60

xxv. SELECT "Element5" "Element6" "Pad5" "Pad6" "Imped5" "Imped6"

xxvi. ROTATE Axis:Z Angle:60

xxvii. SELECT "Element6" "Pad6" "Imped6"

xxviii. ROTATE Axis:Z Angle:60

(e) Now we have monopole elements, their impedance pads (which we will define later) and the ground plane. However, must first subtract the pads from the ground plane so that the ground plane might not short them out.

    i. SUBTRACT "Ground" "Pad" "Pad1" "Pad2" "Pad3" "Pad4" "Pad5" "Pad6"

(f) **Must now make a backing for the feed element**

    i. COORDINATES $x = 0$, $y = 0$, $z = 0$

    ii. CYLINDER Axis:Z Radius:2.31 Height:-5 Segments:12 Name:Backing Color:Blue

    iii. SELECT "Backing"

    iv. ROTATE Axis:Z Angle: 15 degres

(g) **We now immerse the antenna in the air**

    i. COORDINATES $x = 0$, $y = 0$, $z = -70$

    ii. CYLINDER Axis:Z Radius:100 Height:140 Segments:30 Name:Air Color:Red

(h) **Save and Exit**

3. Go to Setup Materials

    (a) MATERIAL ASSIGN "Air" Air

    (b) MATERIAL ASSIGN "Backing" Perfect Conductor

    (c) MATERIAL ASSIGN "Element" Perfect Conductor

    (d) MATERIAL ASSIGN "Element1" Perfect Conductor

    (e) MATERIAL ASSIGN "Element2" Perfect Conductor

    (f) MATERIAL ASSIGN "Element3" Perfect Conductor

    (g) MATERIAL ASSIGN "Element4" Perfect Conductor

    (h) MATERIAL ASSIGN "Element5" Perfect Conductor

    (i) MATERIAL ASSIGN "Element6" Perfect Conductor

    (j) Exit an Save

4. Go to Setup Boundaries

    (a) Select all "Ground" faces as: Boundary $\rightarrow$ Perfect E

    (b) Select top face of "Backing": Source $\rightarrow$ Port $\rightarrow$ WavePort

    (c) Select the face of "Imped1" as: Boundary $\rightarrow$ Lumped RLC

       • View $\rightarrow$ Fit Selection

       • Resistance:0 Inductance: 0 Capacitance:7.11911e $- 13$ % --90 *Ohms*

- Edit Line → Set ... Other → Edge Center OK Click on the center of edge of the rectangle which is shared with the element Enter Click on the center of the edge of the rectangle which is shared with the pad Enter Assign

(d) Do the same for all other Impedance rectangles with capacitances $6.4e^{-5}, 6.4e^{-5}, 6.4e^{-5}, 6.4e^{-5}, 6.4e^{-5}$ for Imped 2,3,4,5 and 6 respectively. % $10^{-6}Ohms \simeq 0Ohms$

(e) Select all faces of "Air" as: Boundary → Radiation

(f) Save and Exit

5. Got to Setup Solution

(a) Select 2.484GHz 20 Passes 50% tetrahedra refinement

6. Click on Solve

7. Pot your Directivity radiation patterns.

Appendix 2: Procedure for Refinement, Obtaining the Far Field Directivity Pattern and Getting the Current Values on the ESPAR Structure Using HFSS

Refinement

Here is the step by step procedure for Refining the ESPAR structure **once it has been solved**. The refinement is very useful is you need to get highly accurate field solutions, for instance to get far field directivity patterns in omni cases where the curve is supposed to be perfectly circular (symmetrical). The refinement requires many time to compile, so I advise you to use it only when really needed. For instance, for a project like a 30°-beam, to refine from 20.000 tetrahedrae to 100.000 tetrahedrae, 8 hours are needed!

Steps:

1. **Setup Solution...**

   Select "Setup Solution..." from the Main menu

   (a) In order to avoid to be stopped by another criterion than the number of tetrahedrae reached, we use the following values: Max Delta S = 0.0002, Tet. Ref. = 50%, Request Passes = 30

   (b) We open the Mesh3D Window:

      i. Mesh Option → Manual Mesh → Define Manual Mesh
      ii. SELECT the object "Air"

    iii. Refine → Object Face → By Volume
- Max Number of elements to be added: 60 000.
- OK button

    iv. Save

    v. Exit the Mesh3D window

(c) Click **OK** to Exit the Setup Solution window

2. **SOLVE**

GETTING FAR FIELD DIRECTIVITY PATTERN WITH HFSS

Steps:

1. **Post Process → Field...**

   Select "Post Process" from the Main menu and choose "Field..." (It may takes some time to open the window.)

   (a) Radiation → Compute → Far Field...

   (b) We want the azimuth antenna pattern[1]:

       i. Phi ranges from -180 to 180 by 300 steps (value used with Matlab programs, see Appendix 3)

       ii. Theta ranges from 90 to 90 by 0 steps (azimuth antenna pattern, $z = 0$)

       iii. OK button
   - In the Plot Far Field pattern window, choose: Quantity = Antenna Directivity Pattern, Polarization = Total
   - Select "Normalize", UnSelect "dB"
   - Choose "Sphere", "2D Polar"
   - **First,** Click on • Phi, and "Select All"
   - **Then,** Click on • Theta, and "Select All" (if not in this order, an error occurs when computing the graph...)
   - OK Button

       iv. Plot → Save As → 2D Plot

       v. Enter "DirectPatternHFSS.dat" (name used in the MAtlab program, see Appendix 3)

   (c) Click **OK** to Exit

GETTING THE CURRENT VALUES USING HFSS

The current values are computed from the H field on a circle around the element at the wanted height, as shown in equation1.2. The circle is drawn with a radius as small as possible, so that the integration loop is as close as possible to the element.

$$\mathbf{I} = \oint \mathbf{H} \bullet dl, \tag{1.2}$$

where $\mathbf{H}$ is the Magnetic field, and dl is the integration loop. $\mathbf{H}$ and $\mathbf{I}$ are complex quantities. Therefore, the evaluation has to be made separately on the real and on the imaginary parts of $\mathbf{H}$ to obtain the real and then the imaginary parts of $\mathbf{I}$. More explanation are available on HFSS on-line help[15].

Here is the explanation on how to get the Magnitude and Phase of the current on element number 1, for the height of $z = 0.01mm$. Firstly, we describe how to draw the circle where the H field will be integrated. Secondly, we explain how to use HFSS 3D Post Process Calculator to get the Amplitude and Phase values.

Steps:

1. **Firstly, we draw the circle:**

   (a) Geometry $\rightarrow$ Create $\rightarrow$ Line
      i. $x = 29.2$ $y = 0$ $z = 0.01$ Number of Points:1000 Name:Circle1H=0 (element number 1, height number 0)[6]
      ii. Change "Straight" into "**Arc**"
      iii. Enter button
      iv. $x = 31.2$
      v. Enter button
      vi. $x = 29.2$
      vii. Enter button
      viii. Done button

2. **Secondly, we use the Calculator to get the currents:**

   (a) Click on the Calculator icone (first one in the icone bar) or choose Data $\rightarrow$ Calculator
      i. Qty $\rightarrow$ H
      ii. Cmplx $\rightarrow$ Real
      iii. Geometry $\rightarrow$ Line $\rightarrow$ Circle1H=0

---

[6]number of element $\epsilon[0..6]$, number of height $\epsilon[0..40]$

    iv. Tangent button

    v. $\int$ button

    vi. Eval button

    vii. Cmplx $\rightarrow$ CmplxR

    viii. Qty $\rightarrow$ H

    ix. Cmplx $\rightarrow$ Imag

    x. Geometry $\rightarrow$ Line $\rightarrow$ Circle1H=0

    xi. Tangent button

    xii. $\int$ button

    xiii. Eval button

    xiv. Cmplx $\rightarrow$ CmplxI

    xv. Exch button

    xvi. Pop button

    xvii. + button

    xviii. Push button

    xix. Cmplx $\rightarrow$ CmplxMag

    xx. Write... button. Enter "m0"

    xxi. Enter "Mag1H=0.reg"

    xxii. Exch button

    xxiii. Cmplx $\rightarrow$ CmplxPhase

    xxiv. Write... button. Enter "p0"

    xxv. Enter "Phase1H=0.reg"

As this is a long and fastidious work, I made 2 macro files: one that automatically draws 41 circles on each element of the ESPAR antenna, and the other one that calculates the values on these circles. These macros are available in RPC285/C:/ProjetsHFSS/ProjetsRPC285/Beam2.pjt/postfld3, respectively named *definecircles40.mac* and *calccourants40.mac*. To execute them one by one, go into the 3d Post Process Field window, and Enter "Ctrl | F3". It may take some time (20 minutes?) to compute those 7 elements × 41 heights × 2 (Amplitude+Phase) = 574 files !

MATLAB EWV APPROXIMATION COMPUTATION

The following step to compute the EWV approximation is to transfer those 574 files and the far field directivity pattern file *DirectPatternHFSS.dat* into the Work directory used by Matlab (in RPC03/D:/MATLABR11/Work/Omni for instance if the Omni case is studied).

    I called:

- Beam2 the 0°-beam,

- Beam3 the 60°-beam,

- Beam4 the 120°-beam,

- Beam5 the 1800°-beam,

- Beam6 the 240°-beam,

- Beam7 the 300°-beam,

- Beam8 the 30°-beam,

using the set of reactances described in table3.1.

Note: The multiple of 60° (0°,60°, ..., 300°) are first, then the multiple of 30° (only 30° in our case, but it can be improved to other set of reactances...).

Therefore, these 475 files corresponding to the input data of a particular set of reactances (omni or beam) have to be saved in the appropriate folder: either Work/Beam2, or Work/Beam3, ..., Work/Beam8 or Omni.

The first parameter of the function *CompSimExp.m* correspond to the number of points picked up per element to compute the EWV appproximation ($NbCircle$[1...41]), that is to say the number of circles where the integration is calculated and the summed.

The second parameter indicates which pattern is calculated: 1 for Omni case, 2 for Beam2 case (0°), 3 for Beam3 case (60°), ..., 7 for Beam7 case (300°), 8 for Beam8 case (30°).

When using the parameter "hfss", the *CompSimExp.m* function uses these files to compute a new file where both HFSS directivity pattern and approximated pattern are recorded. Cross correlation coefficient is also calculated between those 2 patterns using the function *CrossCorrel.m* available in Appendix 4.

.

APPENDIX 3 : MATLAB SOURCE CODES

CompSimExp.m

```
program name : CompSimExp.m
path: Work/CompSimExp.m
comments : Function CompSimExp
```

```
% -------------------------------------------------------------%
%            APPENDIX 2
% -------------------------------------------------------------%
%
%
%
%  Computation of far-field pattern with Equivalent Weigth
%     Vector Approximation from HFSS currents
%
% PARAMETERS:
%  IN:   nbCircle=1..31
%        Pattern=1..8 (1=Omni,2=beam2,etc..,7=Beam7,8=Beam 30 degres)
%        TaillePhi='hfss'(HFSS pattern),'nf'(experimental reactive near field),'ffo'(omni far
%                   field),'ffb'(beam far field)
%  OUT: Cross Correlation coefficient between EWV (sum currents on circles) and HFSS pattern
%
% OUTPUT FILE:
%     Results.txt
%
%
%
%  Author: Helena Jacob
%  July 2002
%
%
% -------------------------------------------------------------%
```

```
function [Res] = CompSim_Exp(nbCircle,Pattern,TypePattern)
%nbCircle=41;
%Pattern=1;
%TypePattern='hfss';

% N*7+2 Input files: Mag0_0.reg, Mag1_0.reg, etc... Mag6_0.reg -> current Magnitudes obtained
%                       on the 7 elements H=0.01mm
%                    Phase0_0.reg, Phase1_0.reg, etc... Phase6_0.reg -> current Phases obtained
%                       on the 7 elements H=0.01mm
%                    ...
%                    Mag0_10.reg, Mag1_10.reg, etc... Mag6_10.reg -> current Magnitudes obtained
%                       on the 7 elements H=14.8mm
%                    Phase0_10.reg, Phase1_10.reg, etc... Phase6_10.reg -> current Phases
%                       obtained on the 7 elements H=14.8mm
%                    ...
%                    Mag0_20.reg, Mag1_20.reg, etc... Mag6_20.reg -> current Magnitudes obtained
%                       on the 7 elements   H=29.59mm
%                    Phase0_20.reg, Phase1_20.reg, etc... Phase6_20.reg -> current Phases
%                       obtained on the 7 elements H=29.59mm

%                    DirectPatternHFSS.dat -> to format it into readable file with kaleidograph
%                    phi301.txt  -> to calculate pattern on 301 points


% 2+N Output files: {resultCurrents0.txt -> current magnitudes and phases obtaines on 7 elements
%                       H=0.01mm
%                    ...
%                    resultCurrents10.txt -> current magnitudes and phases obtaines on 7 elements
%                       H=14.8mm
%                    ...
%                    resultCurrents20.txt -> current magnitudes and phases obtaines on 7 elements
%                       H=29.59mm}
%
%                    { outputFich.txt -> Result of Equivalent Vector approximation }
%                    Results.txt -> result of far-field pattern obtained by HFSS post-process


%-------------------------------------------------------------------------------------------------
%
%            Definition of "TaillePhi"
%                    To get the right phase Phi for the EWV computation
%-------------------------------------------------------------------------------------------------


switch (TypePattern)
  case 'hfss'
   TaillePhi=301;
  case 'nfo' %near field omni
   TaillePhi=601;
```

```
  case 'nfb' %near field beam
   TaillePhi=601;
  case 'ffo' %far field omni
   TaillePhi=682;
  case 'ffb' %far field beam
   TaillePhi=697;
  otherwise
   TaillePhi=0
  end

%_____
%
%           Definition of "folder"
%                   To get the folder where are the hfss currents resulting files
%_____


if (Pattern==1)
   folder=sprintf('Omni');
else
   folder=sprintf(strcat('Beam',Pattern+48));
end


%_____
%
%           Definitions of constants and vectors
%_____

% constant
FRE=2.484*10^9;
LAMDA=3*10^8/FRE;
BATA=2*pi/LAMDA;
% gap between element
D=LAMDA/4;

nbElement=7;
%nbCircle % N

% sterr bector
ASF=zeros(1,nbElement); % (1,7)
% measured current
I7=zeros(nbElement,nbCircle); % (7,21)


%fid_data=zeros(1,nbCircle);
fid_i=zeros(nbCircle,2*nbElement);

IIMag=zeros(nbCircle,nbElement);
```

```
IIPhase=zeros(nbCircle,nbElement);

sol=zeros(1,TaillePhi);
solIigusa=zeros(1,TaillePhi);




%-----------------------------------------------------------------------------------------------
%
%               Reading of the currents calculating by HFSS in files
%                     mag0_0.reg,   ... mag6_40.reg
%                     phase0_0.reg, ... phase6_40.reg
%-----------------------------------------------------------------------------------------------

for k=1:nbElement
    l=k-1; % number of the element
    for j=1:fix(nbCircle/2)
      s=j-1; % number of the circle
      if ((s>=0)&(s<10))
        fid_iMag(j,k)=fopen(strcat(folder,'\Mag',48+l,'_',48+s,'.reg'),'r');
        fid_iPhase(j,k)=fopen(strcat(folder,'\Phase',48+l,'_',48+s,'.reg'),'r');
      else
        dix=fix(s/10);
        unit=s-dix*10;
        fid_iMag(j,k)=fopen(strcat(folder,'\Mag',48+l,'_',48+dix,48+unit,'.reg'),'r');
        fid_iPhase(j,k)=fopen(strcat(folder,'\phase',48+l,'_',48+dix,48+unit,'.reg'),'r');
      end
      end
end




for j=1:nbElement
    for k=1:fix(nbCircle/2)
    fgets(fid_iMag(k,j));
    interm1=fscanf(fid_iMag(k,j),'%s',1);
    interm1=fscanf(fid_iMag(k,j),'%g',1);
    IIMag(k,j)=interm1;
    fgets(fid_iPhase(k,j));
    interm2=fscanf(fid_iPhase(k,j),'%s',1);
    interm2=fscanf(fid_iPhase(k,j),'%g',1);
    IIPhase(k,j)=interm2;
    fclose(fid_iMag(k,j));
    fclose(fid_iPhase(k,j));
%     fprintf(fid_data(k),'%0.15g %0.15g\r\n',interm1,interm2);
end
end
```

```
for k=1:nbElement
   l=k-1; % number of the element
   for j=fix(nbCircle/2)+1:nbCircle
     s=j-1; % number of the circle
     if ((s>=0)&(s<10))
        fid_iMag(j,k)=fopen(strcat(folder,'\Mag',48+l,'_',48+s,'.reg'),'r');
        fid_iPhase(j,k)=fopen(strcat(folder,'\Phase',48+l,'_',48+s,'.reg'),'r');
     else
        dix=fix(s/10);
        unit=s-dix*10;
        fid_iMag(j,k)=fopen(strcat(folder,'\Mag',48+l,'_',48+dix,48+unit,'.reg'),'r');
        fid_iPhase(j,k)=fopen(strcat(folder,'\phase',48+l,'_',48+dix,48+unit,'.reg'),'r');
     end
     end
end


for j=1:nbElement
   for k=fix(nbCircle/2)+1:nbCircle
   fgets(fid_iMag(k,j));
   interm1=fscanf(fid_iMag(k,j),'%s',1);
   interm1=fscanf(fid_iMag(k,j),'%g',1);
   IIMag(k,j)=interm1;
   fgets(fid_iPhase(k,j));
   interm2=fscanf(fid_iPhase(k,j),'%s',1);
   interm2=fscanf(fid_iPhase(k,j),'%g',1);
   IIPhase(k,j)=interm2;
   fclose(fid_iMag(k,j));
   fclose(fid_iPhase(k,j));
%    fprintf(fid_data(k),'%0.15g %0.15g\r\n',interm1,interm2);
  end
end



%for j=1:nbElement
%   figure(j)
%   plot(IIMag(:,j))
%end

%----------------------------------------------------------------------------
%
%
%          Calculation of the complex currents calculated with HFSS
%
%
%----------------------------------------------------------------------------
```

```
for j=1:nbElement
  for k=1:nbCircle
    I7(j,k)=IIMag(k,j)*(cos(IIPhase(k,j)*(pi/180))+i*sin(IIPhase(k,j)*(pi/180)));
              % linear and degrees
  end
end


% normalization by central current
for k=1:nbCircle
  I7norm(:,k)=I7(:,k)./I7(1,k);
end

for j=1:nbElement
   I7sum(j,1)=sum(I7norm(j,:));
   I7sumNonNorm(j,1)=sum(I7(j,:));
end

%_____
%
%
%          Calculation of EWV using Iigusa-san's Method
%
%_____



I7sumNonNorm;
setOfReact=[-90 -90 -90 -90 -90 -90]; %beam2 nbCircle=1   / pas 'hfss'
newCurrent = EwvBeta(I7sumNonNorm,setOfReact);

clear IIMag IIPhase I7;


%_____
%
%
%          Reading of the file Phi.txt containing the values of the phase
%                in order to calculate the EWV
%
%_____



cent=fix(TaillePhi/100);
dix=fix((TaillePhi-100*cent)/10);
unit=TaillePhi-100*cent-10*dix;
```

```
fid_phi=fopen(strcat('Phi',48+cent,48+dix,48+unit,'.txt'),'r');

for k=1:TaillePhi
    comi=fscanf(fid_phi,'%g\n',1); % degres
    Phase(k)=comi(1)*(pi/180); % radians
end

%fid_out=fopen('outputFich.txt','w');

%_____
%
%
%            Equivalent Weight Vector Approximation
%
%_____



%fprintf(fid_out,'SHITA  FA  DA\n');
for SHITA=0:0
    for indicePhi=1:TaillePhi
          FA=Phase(indicePhi); % en radians
     %for n=1:682
          %BFA=fscanf(fid_i2,'%g\n',1);
          %FA=BFA*pi/180;
%         for FA=0:pi/300:2*pi
          % sterring vector elements
          ASF(1,1)=1;
          ASF(1,2)=exp(i*BATA*D*cos(SHITA)*cos(FA));
          ASF(1,3)=exp(i*BATA*D*cos(SHITA)*cos(FA-pi/3));
          ASF(1,4)=exp(i*BATA*D*cos(SHITA)*cos(FA-2*pi/3));
          ASF(1,5)=exp(i*BATA*D*cos(SHITA)*cos(FA-3*pi/3));
          ASF(1,6)=exp(i*BATA*D*cos(SHITA)*cos(FA-4*pi/3));
          ASF(1,7)=exp(i*BATA*D*cos(SHITA)*cos(FA-5*pi/3));
          DA=ASF*I7sum;
          DAIigusa=ASF*newCurrent;
          sol(indicePhi)=abs(DA).^2;
          solIigusa(indicePhi)=abs(DAIigusa).^2;

% fprintf(fid_out,'%0.15g %0.15g %0.15g %0.15g\r\n',FA*180/pi,abs(DA001),abs(DA148),abs(DA2959)
    end
end

clear I7sum DA DAIigusa newCurrent ASF;


fclose(fid_phi);
%fclose(fid_out);
%for k=1:nbCircle
```

```
%  fclose(fid_data(k));
%end

sol=sol/max(sol);  % normalization
solIigusa=solIigusa/max(solIigusa);

%_____
%
%
%           Read DirectPatternHFSS.dat (far field pattern from HFSS) and format it into
%                    Results.txt readable with kaleidagraph
%
%_____

switch(TypePattern)
  case 'hfss'

    fid_i=fopen(strcat(folder,'\DirectPatternHFSS.dat'),'r');
    fid_out=fopen('Results.txt','w');

    tailleTitre=6;

    for k=1:tailleTitre
    fgets(fid_i);
    end


    for k=1:TaillePhi
      interm1=fscanf(fid_i,'%g',1);
      interm2=fscanf(fid_i,'%g',1);
      fprintf(fid_out,'%0.15g %0.15g %0.15g\r\n',interm1,interm2,sol(k));%Iigusa(k));%
    end

    fclose(fid_i);
    fclose(fid_out);
%_____
%
%
%           To Calculate cross correlation coefficient between HFSS far field pattern
%                 and EWV
%
%_____


%_____
%
%
%           Write in Results.txt values of EWV versus the chosen experimental Phase ('near field,
%                 far field omni, fear field beam') readable with Kaleidagraph
```

```
%--------------------------------------------------------------------------------

otherwise

  fid_out=fopen('Results.txt','w');


  for k=1:TaillePhi
    FA=Phase(k); % en radians
    fprintf(fid_out,'%0.15g %0.15g %0.15g\r\n',FA*180/pi,sol(k),solIigusa(k));
  end

  fclose(fid_out);

end

Res=CrossCorrel(TaillePhi,'Results');
```

APPENDIX 4 : MATLAB SOURCE CODES

CrossCorrel.m

program name : CrossCorrel.m
path: Work/CrossCorrel.m
comments : Function CrossCorrel

```
% -------------------------------------------------------------%
%               APPENDIX 2
% -------------------------------------------------------------%
%
%
%
% Cross correlation between two patterns
%
% PARAMETER:
%     TaillePhi=301(HFSS pattern),601(experimental reactive near field),682(omni far field),
%              697(beam far field)
%     file= [?].txt: Column  Data
%                       1     PhaseA
%                       2     Da
%                       3     Df


function Res=CrossCorrel(Taille,file)

% File Pattern.txt: Column  Data
% 1 PhaseA
% 2 Da
% 3 Df


%Taille=601;
```

73

```
PhaseA=zeros(1,Taille);
Da=zeros(1,Taille);
Df=zeros(1,Taille);

fid_i=fopen(strcat(file,'.txt'),'r');

for j=1:Taille
    comi=fscanf(fid_i,'%g %g %g\n',3); %'%g %g\n',2); %
    PhaseA(j)=comi(1);
    Da(j)=comi(2);
    Df(j)=comi(3);
end

%Df=ones(1,Taille);

Da=Da.*exp(i*PhaseA);
Df=Df.*exp(i*PhaseA);

rho=(sum(Da.*conj(Df)))/sqrt(sum(abs(Da).^2)*sum(abs(Df).^2));


fprintf('%0.6g\r\n',abs(rho));

Res=abs(rho);

fclose(fid_i);
```

APPENDIX 5 : MATLAB SOURCE CODES

Capa.m

```
program name : Capa.m
path: Work/Capa.m
comments : Function Capa
```

```
% -------------------------------------------------------------%
%                 APPENDIX 2
% -------------------------------------------------------------%
%
% To calculate from the bias voltage (-2048,2047) value or the
% reactance value (-4.7684 Ohms, -93.6299 Ohms), the capacitance value used in
% HFSS Simulation (1.34368e-11 F, 6.84311e-13 F)
%
% Capa(In,TypeIn)
% if TypeIn='v', input is Bias voltage
% if TypeIn='x', input is Reactance value
%
% Author: Helena JACOB
%   August 2002
% -------------------------------------------------------------%


function res=Capa(In,TypeIn)


f0=2.484e9;

switch (TypeIn)

    case 'v'
    Xi=(-0.0217*In-49.21)
```

```
  case 'x'
    Xi=In;
end

Res=-1/(2*pi*f0*Xi);

fprintf('%0.8g\r\n',Res);
```

Appendix 6 : IEICE Paper

Ground Skirt Monopole Array Antenna Far Field Analysis Based on an Equivalent Weight Vector Approximation

H. Jacob, Q. Han, K. Inagaki, and T. Ohira

ATR Adaptive Communications Research Laboratories

1. Abstract

This paper presents a new technique in which a ground skirt monopole array antenna far field is analyzed based on an Equivalent Weight Vector (EWV) approximation. We computed the far field patterns from current only at discrete points picked up on the ground skirt monopole array antenna rather than electromagnetic field on the entire radiation boundary of the antenna. Results obtained based on EWV approximation are compared with those obtained from Finite Element Method (FEM) [1]. As a result, cross correlation coefficients are 0.9999 for omni pattern and 0.9856 for beam pattern between the results obtained by EWV and FEM.

2. Ground Skirt Monopole Antenna

Figure 1 shows a 7-element ground skirt monopole antenna consisting of a center feed element and 6 surrounding parasitic elements with varactors at their bases. Variable reactances of the varactors, controlled by bias voltages, alter the performance of the antenna so that directional beams can be steered through 360° azimuth. Frequency of the antenna is 2.484 GHz (λ=12.07 cm). All the elements are slightly shorter than 0.25λ mounted on a circle ground with a radius of 0.5λ to obtain resonance at the desired frequency. A skirting is used on a finite ground plane structure to reduce the main lobe elevation [2].
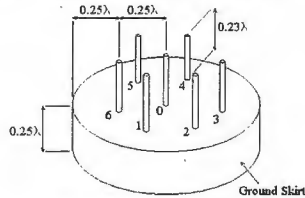

Fig. 1 ESPAR antenna structure

3. Far-field Analysis Based on EWV Approximation

Rigorously speaking, antenna far field patterns are obtained by integrating electromagnetic components on a closed surface of an antenna,

$$E(x,y,z) = \int_S \left(\left(j\omega\mu_0 H_{tan} \right)G + \left(E_{tan} \times \nabla G \right) + \left(E_{normal} \nabla G \right) \right)ds \quad (1)$$

where, $E(x,y,z)$ and S represent the electric field and the radiation boundary surface, respectively. In Eq. (1), subscript $_{tan}$ and $_{normal}$ mean tangential and normal component of the magnetic and electric fields, respectively. And G is the free space Green's function and μ_0 is the free space relative permeability. It is evident that a great many points have to be measured or computed to get a far field pattern by using (1). As a result, a far field analysis of even a small antenna would cost great time. Therefore, a method based on EWV approximation in which the far field patterns are calculated from the current only at discrete points is proposed. The far field directivity pattern of current-based antenna is calculated by using the following equations,

$$D_a(\theta, \varphi) = i^T a \quad (2)$$

$$i = \left[i_0, i_1, ..., i_n \right]^T, \quad a = \left[a_0, a_1, ..., a_n \right]^T,$$

$$a_k = \exp\left[j\beta r_k^T \left[\cos\theta\cos\phi, \cos\theta\sin\phi, \sin\theta \right]^T \right],$$

where, $D_i(\theta, \varphi)$ represents array factor, i equivalently plays the role of weight vector of the array antenna, a is the array' steering vector, r_k (k=0 to n) is the position vector, θ and φ are the azimuth and elevation angle, respectively.

4. Results and Comparison

We, firstly, analyze the ESPAR antenna by simulating the model shown in Fig. 1 using FEM, and, then using EWV approximation. Figure 2 shows the results of both omni and beam far field patterns. The solid lines, in the Fig. 2, represent the EWV results and the dashed lines represent FEM results. For the omni pattern, a good agreement is obtained, while for the beam pattern, there is some difference exhibits. To evaluate the difference, we also calculate cross correlation coefficients between the results obtained by EWV and the FEM and they are 0.9999 for omni pattern and 0.9856 for beam pattern.

5. Conclusion

A ground skirt monopole array antenna far field was analyzed based on an Equivalent Weight Vector approximation. The results were compared with those obtained by Finite Element Method. The cross correlation coefficients between the results obtained by EWV and the FEM were also calculated and were 0.9999 for omni pattern and 0.9856 for beam pattern. Therefore, we conclude that EWV approximation is effective to analyze the far field pattern for current-based array antenna.

References
[1] http://www.ansoft.com June 2002.
[2] Y. Ojiro, et.al. "Improvement of Elevation Directivity for Espar Antennas with Finite Ground Plane", IEEE AP-S International Symp. Boston, July 2001.
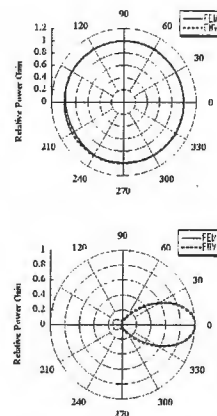
Fig. 2 Omni and beam patterns calculated by FEM and EWV